General Disclaimer

One or more of the Following Statements may affect this Document

- This document has been reproduced from the best copy furnished by the organizational source. It is being released in the interest of making available as much information as possible.

- This document may contain data, which exceeds the sheet parameters. It was furnished in this condition by the organizational source and is the best copy available.

- This document may contain tone-on-tone or color graphs, charts and/or pictures, which have been reproduced in black and white.

- This document is paginated as submitted by the original source.

- Portions of this document are not fully legible due to the historical nature of some of the material. However, it is the best reproduction available from the original submission.

Produced by the NASA Center for Aerospace Information (CASI)

ACOUSTIC SCATTERING BY A POROUS ELLIPTIC CYLINDER WITH NONLINEAR RESISTANCE

By

William Edward Zorumski

Thesis submitted to the Graduate Faculty of the

Virginia Polytechnic Institute

in candidacy for the degree of

DOCTOR OF PHILOSOPHY

in

Engineering Mechanics

APR 1971
RECEIVED
NASA STI FACILITY
INPUT BRANCH

FACILITY FORM 602
N71-21408
(ACCESSION NUMBER)
(THRU)
109
(PAGES)
G3
(CODE)
TMX 67019
(NASA CR OR TMX OR AD NUMBER)
23
(CATEGORY)

March 1970

ACOUSTIC SCATTERING BY A POROUS ELLIPTIC CYLINDER WITH NONLINEAR RESISTANCE

by

William Edward Zorumski

Thesis submitted to the Graduate Faculty of the

Virginia Polytechnic Institute

in partial fulfillment for the degree of

DOCTOR OF PHILOSOPHY

in

Engineering Mechanics

APPROVED:

Chairman, Dr. Jerry Counts

Dr. R. Thomas Davis

Dr. Richard P. McNitt

Dr. Dean T. Mook

Dr. George A. Gray

March 1970

Blacksburg, Virginia

ACOUSTIC SCATTERING BY A POROUS ELLIPTIC CYLINDER

WITH NONLINEAR RESISTANCE

By

William Edward Zorumski

ABSTRACT

Equations for high intensity acoustic waves are derived from the general equations governing a compressible isotropic Newtonian fluid. The integral conservation laws of continuum mechanics are used to determine a general set of laws, similar to shock wave relations, which describe the interaction of these waves with thin porous sheets of material. A special case of these laws, where the velocity normal to the sheet is continuous and the pressure drop across the sheet is a nonlinear function of the normal velocity, is used to study acoustics problems with nonlinear material effects. Numerical, approximate, and exact solutions are obtained from the one-dimensional problem where two regions are coupled through a porous sheet with nonlinear resistance.

Solutions for scattering from a thin rigid porous elliptic cylindrical shell are found in terms of Mathieu functions. When the acoustic resistance of the shell is linear and constant, the scattering problem reduces to an infinite set of linear equations for the coefficients of the velocity expansion on the cylinder. Coupling terms in these equations are given by integrals involving Mathieu functions which are evaluated by exact methods. A special case of variable linear resistance is found where the infinite systems uncouple so that closed form solutions may be found for the velocity coefficients. Computations are

made in the intermediate frequency range, where the wavelength is of the same order of magnitude as the major axis of the cylinder. Tabulations of the scattered and dissipated energies are given for various cylinder eccentricities, resistances, incidence angles, and frequencies. A perturbation solution is given for scattering from a cylinder with slightly nonlinear resistance. This solution is used to obtain the scattering of intense sawtooth waves from a cylinder with nonlinear resistance.

ACKNOWLEDGMENTS

The author wishes to express his appreciation to his advisor, Dr. J. Counts, for exerting that extra effort which is required to guide research outside of one's personally preferred area, and for his continuous encouragement.

Credit is due to Mr. Donald Lansing at Langley Research Center, NASA, for his continued interest in this work and for his invaluable aid in areas of mathematics. Mrs. Edith McNeill and Mrs. Yvonne Powell have done an excellent typing job in record time and the author is grateful for this work.

Since life in graduate school has been a family endeavor, the author dedicates this thesis to Olivia, Joe, and Barry.

TABLE OF CONTENTS

SECTION		PAGE
I.	INTRODUCTION	1
II.	DERIVATION OF EQUATIONS AND BOUNDARY CONDITIONS	10
III.	THE ONE-DIMENSIONAL PROBLEM	22
IV.	SCATTERING FROM A POROUS ELLIPTIC CYLINDER	41
V.	RESULTS AND DISCUSSION	66
VI.	CONCLUDING REMARKS	88
VII.	BIBLIOGRAPHY	91
VIII.	VITA	96
IX.	APPENDIX: EVALUATION OF COUPLING COEFFICIENTS	97

LIST OF FIGURES

FIGURE		PAGE
1.	Flow through porous element	17
2.	Pressure drop functions for typical material.	24
3.	One-dimensional problem for two regions coupled through a nonlinear porous sheet.	27
4.	Waves reflected from a porous sheet with nonlinear resistance.	36
5.	Elliptical coordinates.	42
6.	Pressure drop function for typical fiber glass plastic porous material	67
7.	Velocity amplitude predicted by exact and approximate solutions	69
8.	Comparison of dissipation by elliptic cylinder and parallel planes	82
9.	Grazing incidence scattering of a sawtooth wave.	84
10.	Velocity amplitude at cylinder surface for grazing wave . .	86
11.	Normal incidence scattering of a sawtooth wave	87

LIST OF TABLES

TABLE		PAGE
I.	Relation Between Perturbation Parameter and SPL	23
II.	Scattered and Dissipated Power Ratios, h = 2.0	76
III.	Scattered and Dissipated Power Ratios, h = 4.0	77
IV.	Scattered and Dissipated Power Ratios, h = 6.0	78
V.	Scattered and Dissipated Power Ratios, h = 8.0	79
VI.	Scattered and Dissipated Power Ratios, h = 10.0	80

I. INTRODUCTION

The idealized problem of scattering from a porous cylinder originates from the contemporary need for methods to reduce noise from aircraft turbofan engines. In reference 1, Marsh has shown that a practical method for reducing discrete-tone noise from turbofan engines is to install "broad-band resonators" inside the engine nacelle. Because of considerations of weight, safety, and endurance, these resonators are usually made of thin porous sheets of material (either metallic or fiberglass-plastic) which are fastened to a compartmented wall. The cavities behind the porous sheet are usually about one-quarter wavelength in depth, since this gives good absorbing qualities.

In general, the greater the exposed area of porous material, the more sound is absorbed, so that engine designers must look for ways to alter the engine geometry to increase this area. Of course, this must be accomplished without upsetting the basic flow field within the engine, which presumably has already been optimized on a performance basis. One approach to this problem has been to install thin porous double-walled radial spokes or circumferential rings in the engine. The optimum size (from the acoustical viewpoint) of these devices is not known, but it is reasonable to assume that their dimensions are of the same order of magnitude as the wavelength of the dominant tone. In cross section, such a spoke or ring would appear roughly as an ellipse. This suggests that their qualities may be

evaluated by studying the two-dimensional problem of scattering from a porous elliptical cylinder.

Measured data in a typical engine indicate that the acoustic intensity is of the order of 160 dB. This corresponds to a pressure fluctuation of about one-hundredth of an atmosphere. There is some debate among investigators as to whether this intensity is in the linear range (where the classical wave equation is valid) or in the nonlinear range (where some more exact set of equations must be used). The fact is that this question may not be answered in terms of a statement about acoustic intensity. Acoustic equations are perturbation equations of the general Newtonian fluid equations, and each problem must be judged on its own merits as to whether it is a linear or nonlinear problem. As evidence of this, several important papers on nonlinear acoustics are mentioned here, although no attempt is made to survey this area of research.

In one of the earlier papers (omitting Lord Rayleigh) Fay (ref. 5) obtained a Fourier Series solution to the one-dimensional wave equation in an unbounded medium. His equations considered a nonlinear compressibility law (adiabatic) which causes wave peaks to travel faster than wave troughs. A viscosity term in the equations limited the shape from continued steepening. He concluded that there is no completely stable wave, but that there is a "nearly stable" wave whose shape changes gradually. In reference 6, Fubini gives a solution to a nonlinear one-dimensional problem which, like Fay's, has nonlinear compressibility, but which does not consider viscosity.

His solution, which is given as a series of Bessel functions, predicts that a discontinuity will form in the wave. More recently Blackstock (ref. 4) has generalized the work of Fay and Fubini. His work shows that the Fubini solution is valid near the source, and the Fay solution is valid far from the source. Using a weak-shock approach, Blackstock has obtained a general solution which is also valid in the transition region between near and far field. The perturbation approach has been used by Coppens and Saunders in reference 7 to obtain a finite-amplitude standing wave solution in a rigid-walled tube of finite length. Experiments made by them confirm theoretical computations for second and third harmonics of the fundamental wave. Reference 8 is another example of the use of perturbation equations for nonlinear equations. In this work, Maslen and Moore investigate strong transverse waves in a circular cylinder. The surprising thing about their investigation is their prediction that strong transverse waves will be shock free, in contrast to the plane wave case where shocks form.

Isakovich, in reference 9, presents a discussion of a Sturm-Lioville problem obtained from the one-dimensional wave equation. He also concludes that second-order terms in these problems will always be bounded.

For the reader intersted in surveying the area of nonlinear acoustics, the book by Morse and Ingard (ref. 5), and Beyer's survey in Chapter 10 of Mason's "Physical Acoustics" (ref. 2), are recommended as a place to start.

The nonlinearity which arises from the boundary conditions of the problem (rather than from the governing differential equations) will be the focus of attention in the present work. This nonlinearity is a characteristic of the porous material. It must be mentioned, however, that no time will be spent in detailed consideration of flow and wave motion in the porous media. This is a complex subject in itself, but it has been developed to a fairly refined state, primarily through the efforts of Biot (refs. 10 and 11). In the following discussion, only very thin sheets of the porous materials will be considered, so that their properties may be characterized by functions which represent the changes in flow parameters from one side of the sheet to the other. The situation here is analogous to shock wave equations, where relations are obtained for computing the discontinuities in flow parameters at the shock wave.

The problem of interaction of flow with screens or grids is important in a number of applications. For example, references 12 and 13 consider flows through grids of heat exchangers. Screens are used for smoothing flows in wind tunnels (refs. 14 and 15), and for protecting aircraft engines (ref. 16). These studies were primarily concerned with evaluation of a pressure loss coefficient. Reference 17 is an analytical and experimental study of a strong wave interaction with a wire grid. In this research, Center studied a centered rarefaction wave as it impinged on the screen. He assumed:

(a) quasi-steady flow near the grid

(b) no heat transfer in the fluid or between the grid and fluid

(c) effect of grid represented by a drag coefficient which depends only on Mach number

With these assumptions, good agreement was found between theory and experiment.

The theory of dimensional analysis suggests that the drag coefficient used by Center should depend on both the Reynolds and the Mach number. Careful steady flow investigations by Yates (ref. 18) and by Pinker and Herbert (ref. 19) have experimentally confirmed this fact. These authors measured coefficients for flows (inside the porous screens) varying from laminar, through turbulent, to choked flow. Both investigations show a dependence on Reynolds' number, but the strongest dependence could be associated with Mach's number, which is apparently why Center's assumption was adequate in his problem.

All of the research on screens mentioned above was concerned with Mach numbers which are fairly large compared to those found in acoustical work where a "large" Mach number would be of the order of 0.1. Work in acoustics has concentrated on perforated plates, or more specifically, on plates with a single perforation, that is, an orifice. Also, almost all work in this area has been carried out using impedance ideas. These ideas originated in discrete electrical and mechanical systems and are limited to linear, steady-state problems. In spite of this, the tradition in acoustics has been to

account for nonlinearity by a modification of the impedance concept, which results in a quasi-linear theory.

In 1935, Sivian conducted an experimental investigation of the impedance of an orifice (ref. 20). He concluded that the reactance of the orifice was only slightly dependent on amplitude (of an incident sound wave), but that the resistance increased with amplitude. Sivian's work was followed by Ingard in reference 21, who concluded that resistance increases and reactance decreases with amplitude. Bies and Wilson made an unsuccessful attempt in 1957 (ref. 22) to resolve differences between the work of Sivian and Ingard. Also in 1957, Thurston, Hargrove, and Cook (ref. 23) made the first investigation of coupling between waves of different frequencies due to the nonlinear behavior of an orifice. Their study was of steady flow (zero frequency) coupled with a single harmonic wave. Reference 24 is a recent investigation of the same coupling phenomenon by Ingard and Ising. No investigations have been made to date of coupling between one or more nonzero frequency waves striking an orifice or other resistive element with nonlinear characteristics. Such investigations would be nearly futile if the empirical quasi-linear impedance approach were used, because of the infinite number of amplitude and frequency combinations which can occur in a nonharmonic wave.

In reference 25, this writer and Parrott presented an acoustical theory for thin porous sheets which, like Center's (ref. 17) work, used a shock-type relation for the screen. This work was the first

break with the traditional impedance approach in acoustics. Experimental work (ref. 25) confirmed that the theory was useful. In this dissertation, a rational derivation of a general acoustic theory for thin porous sheets will be given. Solutions for one-dimensional problems will be obtained from this. Next, the two-dimensional problem of scattering from porous strips and elliptical cylinders will be treated.

The literature on diffraction is extensive. The reader interested in this should consult the important review article by Bouwkamp (ref. 26). This survey reviews more than 500 papers published between 1940 and 1954. The application of Mathieu functions to diffraction problems is discussed in Bouwkamp's article. Briefly, Mathieu's functions may be used in the study of diffraction (or scattering) from elliptic cylinders. His article indicates that research prior to 1954 was limited to the studies of the strip or slit (cylinder with eccentricity 1). This problem has also been studied with an integral equation formulation (ref. 3).

Since Bouwkamp's review, several papers have been published which deal with cylinders having eccentricity less than 1. In 1963, Yeh discussed the problem of a penetrable strip in terms of a Mathieu function series (ref. 27), and Barakat (ref. 28) made a study of the elliptic cylinder with various eccentricities. Barakat considered the exterior problem using the classical Dirichlet (sound soft) and Neuman (sound hard) boundary conditions. This work

made use of recently computed tables by Barakat, Houston, and Levin (refs. 30 and 31). These tables are appropriate for scattering problems in the low-to-medium frequency range. Following Barakat's work, Burke and Twersky (refs. 29, 32, and 33) began investigations using low-frequency approximations.

In reference 29, Burke considered the problem where there is cylinder composed of fluid with a density different from the media in which it is immersed. Boundary conditions at the surface of the elliptic cylinder were continuity of normal velocity and of pressure. His paper, like the one by Yeh (ref. 27), considered the coupled interior and exterior cylinder problems. The analysis of this problem resulted in an infinite set of algebraic equations for the scattered waves. Burke indicated the connection between truncating these sets of equations and low-frequency approximations. His solution gave the far-field scattering amplitude to the sixth power of the wave number, and the near-field (internal and external) to the third power. Terms in the truncated equations could be evaluated either from the previously mentioned tables of Barakat, Houston, and Levin, from Wiltse and King's tables (refs. 34 and 35), or from computations based on known expansions of the Mathieu functions in terms of the other tabulated transcendental functions.

The classical text on the theory of Mathieu functions is McLachlan's work (ref. 36). The best introduction to the subject, however, is probably Arscott's excellent book (ref. 37). The notations are the same in both books, which greatly simplifies

collateral study. Arscott's proofs of the basic theorems and McLachlan's profusion of derived equations, expansions, and identities form a good combination. For the more sophisticated reader, Meixner and Schäfke's (ref. 38) work is available, and brief summaries are given in references 39, 40, 41, and 42. Some tables are also given in reference 40, but reference 42, the National Bureau of Standards Table, is the most extensive table available, being an extended edition of reference 41.

II. DERIVATION OF EQUATIONS AND BOUNDARY CONDITIONS

2.1 Acoustic Wave Equation

A derivation of the wave equation may be found in a large number of papers and texts (refs. 2 and 3). The pertinent equations are rederived here in order to clearly define the range of variables for which they are valid, and to add continuity to this work.

Since acoustics is only a restricted part of the field of fluid mechanics, the equations are derived by a straightforward parameter perturbation of the general equations governing a compressible isotropic Newtonian fluid.

The general equations for a kinetically and calorically perfect gas with constant coefficients of viscosity and conductivity are as follows:

$$p = \rho RT \tag{1}$$

$$\frac{\partial \rho}{\partial t} + (\rho q_i)_{,i} = 0 \tag{2}$$

$$\rho \frac{Dq_i}{Dt} = -p_{,i} + \frac{\mu}{3} q_{j,ji} + \mu q_{i,jj} \tag{3}$$

$$\frac{\partial}{\partial t}\left[\rho\left(\frac{q^2}{2} + C_pT\right)\right] + \left[\rho\left(\frac{q^2}{2} + C_pT\right)q_i\right]_{,i} = \frac{\partial p}{\partial t}$$

$$- \frac{2}{3}\mu\left[q_{k,k}q_i\right]_{,i} + \mu\left[(q_{i,j} + q_{j,i})q_j\right]_{,i} + KT_{,ii} \tag{4}$$

Since only small fluctuations of the fluid state are to be considered, the ambient pressure, density, and temperature, p_o, ρ_o, and T_o, respectively, will be used as reference quantities. A reference length and time are also needed, and for these the reciprocals of circular frequency ω, and wave number, κ, will be used.

Thus, denoting dimensional variables by (*)'s, and dimensionless ones by $(\bar{x})$'s, the following set of dimensionless variables is introduced:

$$x_i^* = \frac{\bar{x}_i}{\kappa} \tag{5a}$$

$$t^* = \frac{\bar{t}}{\omega} \tag{5b}$$

$$q_i^* = \frac{\omega}{\kappa}\,\bar{q}_i \tag{5c}$$

$$p^* = p_o\bar{p} \tag{5d}$$

$$\rho^* = \rho_o\rho \tag{5e}$$

$$T^* = T_o\bar{T} \tag{5f}$$

A few remarks about the above quantities are needed here. The frequency range of interest is of the order of 10^3 Hz, perhaps 100 Hz to 10,000 Hz. Correspondingly, the wave lengths will vary from 35 cm to 0.35 cm and the wave numbers from 0.2 cm^{-1} to 20 cm^{-1}. $\left(\frac{\omega}{\kappa}\right)$ will be roughly the speed of sound, or about 350 meters/sec. Thus, $\bar{q}_1$ is a Mach's number, and will be quite small. $\bar{p}$ is the

pressure fluctuation in atmospheres, which is also assumed to be very small.

The reference pressure, density, and temperature will be chosen to satisfy the perfect gas law.

$$p_o = \rho_o R T_o \tag{6}$$

The dimensional equations will now be converted to dimensionless variables. Equation (1), with the condition of equation (6), is simply

$$\bar{p} = \bar{\rho}\,\bar{T} \tag{7}$$

The continuity equation is of the same form as before, namely

$$\frac{\partial \bar{\rho}}{\partial \bar{t}} + \frac{\partial(\bar{\rho}\bar{q}_i)}{\partial \bar{x}_i} = 0 \tag{8}$$

Equation (3), the momentum equation, contains two parameters after the changes of variable.

$$\bar{\rho}\,\frac{D\bar{q}_i}{Dt} = -\left(\frac{\kappa^2 p_o}{\omega^2 \rho_o}\right)\frac{\partial \bar{p}}{\partial \bar{x}_i} + \frac{\kappa^2 \mu}{\rho_o \omega}\left(\frac{1}{3}\,\frac{\partial^2 \bar{q}_j}{\partial \bar{x}_j\,\partial \bar{x}_i} + \frac{\partial^2 \bar{q}_i}{\partial \bar{x}_j\,\partial \bar{x}_j}\right) \tag{9}$$

The energy equation also brings in two additional parameters. After transformation it is

$$\frac{\partial}{\partial \bar{t}}\left[\bar{\rho}\left(\frac{\bar{q}^2}{2} + \frac{C_p T_o}{\left(\frac{\omega}{\kappa}\right)^2}\,\bar{T}\right)\right] + \frac{\partial}{\partial \bar{x}_i}\left[\bar{\rho}\left(\frac{\bar{q}^2}{2} + \frac{C_p T_o}{\left(\frac{\omega}{\kappa}\right)^2}\right)\bar{q}_i\right] = \frac{p_o}{\rho_o\left(\frac{\omega}{\kappa}\right)^2}\,\frac{\partial \bar{p}}{\partial \bar{t}}$$
$$+ \frac{\mu\kappa}{\rho_o\left(\frac{\omega}{\kappa}\right)}\left\{-\frac{2}{3}\,\frac{\partial}{\partial \bar{x}_i}\left[\frac{\partial \bar{q}_k}{\partial \bar{x}_k}\,\bar{q}_i\right] + \frac{\partial}{\partial \bar{x}_i}\left[\left(\frac{\partial \bar{q}_i}{\partial \bar{x}_j} + \frac{\partial \bar{q}_j}{\partial \bar{x}_i}\right)\bar{q}_j\right]\right\} + \frac{\kappa K T_o}{\rho_o\left(\frac{\omega}{\kappa}\right)^3}\,\frac{\partial^2 \bar{T}}{\partial \bar{x}_i\,\partial \bar{x}_i} \tag{10}$$

Consider the set of parameters which appear in the transformed equations (7) through (10). They are

$$\frac{p_o}{\rho_o\left(\frac{\omega}{\kappa}\right)^2}, \quad \frac{\kappa\mu}{\rho_o\left(\frac{\omega}{\kappa}\right)}, \quad \frac{C_pT_o}{\left(\frac{\omega}{\kappa}\right)^2}, \text{ and } \frac{\kappa KT_o}{\rho_o\left(\frac{\omega}{\kappa}\right)^3}$$

The first term, $\frac{p_o}{\rho_o\left(\frac{\omega}{\kappa}\right)^2}$, is approximately $\frac{1}{\gamma}$.

This is a first order term. The second is an inverted Reynolds number.

$$\frac{\kappa\mu}{\rho_o\left(\frac{\omega}{\kappa}\right)} \cong \frac{2\pi}{\left(\frac{\rho_o c\lambda}{\mu}\right)}$$

This number is of the order 10^{-6} for the wavelengths of interest in air, so that it may justifiably be called a small quantity.

$\frac{C_pT_o}{\left(\frac{\omega}{\kappa}\right)^2}$ is roughly 3 for air, so it must be considered a first-order term. $\frac{\kappa KT_o}{\rho_o\left(\frac{\omega}{\eta}\right)^3}$ varies from about 0.03×10^{-4} to 3×10^{-4}, the larger value corresponding to the larger wave number, or frequency, thus it may be considered to be a small quantity. Using the dimensionless groups discussed above, the following quantities are defined:

$$\frac{p_o}{\rho_o\left(\frac{\omega}{\kappa}\right)^2} = \frac{1}{\gamma}, \quad \frac{\kappa\mu}{\rho_o\left(\frac{\omega}{\kappa}\right)} = \frac{\epsilon}{\overline{N}_{Ra}} \tag{11a,b}$$

$$\frac{C_pT_o}{\left(\frac{\omega}{\kappa}\right)^2} = \overline{C}_p, \quad \frac{\kappa KT_o}{\rho_o\left(\frac{\omega}{\kappa}\right)^3} = \epsilon\overline{K} \tag{11c,d}$$

The new quantities defined in equations (11) may now be thought of as of order 1. If ϵ is not chosen smaller than 10^{-4}, $\bar{N}_{Ra}$ will be roughly 1 or greater, and $\bar{k}$ will be roughly less than 3.

Asymptotic solutions for equations (7) through (10) may be found in the form

$$\bar{p} \sim 1 + \epsilon\bar{p}_1 + \epsilon^2\bar{p}_2 + \ldots \tag{12a}$$

$$\bar{\rho} \sim 1 + \epsilon\bar{\rho}_1 + \epsilon^2\bar{\rho}_2 + \ldots \tag{12b}$$

$$\bar{T} \sim 1 + \epsilon\bar{T}_1 + \epsilon^2\bar{T}_2 + \ldots \tag{12c}$$

$$\bar{q}_i \sim 0 + \epsilon\bar{q}_{i1} + \epsilon^2\bar{q}_{i2} + \ldots \tag{12d}$$

Substituting these asymptotic expansions into the governing equations gives the desired sets of first and second order equations. This is a routine procedure except for equation (10), the energy equation. Here, it must be noted that the leading term in the temperature expansion gives a large reference energy level. Because of the continuity equation, this term drops out of the energy equation. This can be accounted for by substituting $\epsilon\bar{T}_1 + \epsilon^2\bar{T}_2$ into the energy equation, that is, by using a relative temperature.

If this is not done, the resulting prediction would be that the speed of sound is $\sqrt{RT}$, instead of the correct value of $\sqrt{\gamma RT}$. Keeping this in mind, the governing first and second order asymptotic equations may be found. They are as follows:

$$\bar{p}_1 - (\bar{\rho}_1 + \bar{T}_1) = 0 \tag{13a}$$

$$\frac{\partial \bar{\rho}_1}{\partial \bar{t}} + \frac{\partial \bar{q}_{i1}}{\partial \bar{x}_i} = 0 \tag{13b}$$

$$\frac{\partial \bar{q}_{i1}}{\partial \bar{t}} + \frac{1}{\gamma}\frac{\partial \bar{p}_1}{\partial \bar{x}_i} = 0 \tag{13c}$$

$$\bar{C}_p \frac{\partial \bar{T}_1}{\partial \bar{t}} - \frac{1}{\bar{\gamma}}\frac{\partial \bar{p}_1}{\partial \bar{t}} = 0 \tag{13d}$$

$$\bar{p}_2 - (\bar{\rho}_2 + \bar{T}_2) = 0 \tag{14a}$$

$$\frac{\partial \bar{\rho}_2}{\partial \bar{t}} + \frac{\partial \bar{q}_{i2}}{\partial \bar{x}_i} = - \frac{\partial(\bar{\rho}_i \bar{q}_{i1})}{\partial \bar{x}_i} \tag{14b}$$

$$\frac{\partial \bar{q}_{i2}}{\partial \bar{t}} + \frac{1}{\bar{\gamma}}\frac{\partial \bar{p}_2}{\partial \bar{x}_i} = - \bar{q}_{j1}\frac{\partial \bar{q}_{i1}}{\partial \bar{x}_j} - \bar{\rho}_1 \frac{\partial \bar{q}_{i1}}{\partial \bar{t}} + \frac{1}{\bar{N}_{Ra}}\left[\frac{1}{3}\frac{\partial^2 \bar{q}_{j1}}{\partial \bar{x}_j\, \partial \bar{x}_i} + \frac{\partial^2 \bar{q}_{i1}}{\partial x_j\, \partial x_j}\right] \tag{14c}$$

$$\bar{C}_p \frac{\partial \bar{T}_2}{\partial \bar{t}} - \frac{1}{\bar{\gamma}}\frac{\partial \bar{p}_2}{\partial \bar{t}} = - \bar{C}_p\left[\frac{\partial(\bar{T}_i \bar{q}_{i1})}{\partial \bar{x}_i} + \frac{\partial(\bar{\rho}_1 \bar{T}_1)}{\partial t}\right] + \bar{q}_{i1}\frac{\partial \bar{q}_{i1}}{\partial \bar{t}} + \bar{K}\frac{\partial^2 \bar{T}_1}{\partial \bar{x}_i\, \partial \bar{x}_i} \tag{14d}$$

The first order set of equations (13) may now be manipulated to obtain wave equations.

Since
$$\bar{C}_p \bar{\gamma} = \frac{\gamma}{\gamma - 1} \tag{15}$$

the equation

$$\frac{\partial \bar{p}_1}{\partial \bar{t}} = \gamma \frac{\partial \bar{\rho}_1}{\partial \bar{t}} \tag{16}$$

is a direct result of the perfect gas law and the energy equation. With this, we may find the wave equation

$$\frac{\partial^2(\bar{p}_1, \bar{\rho}_1, \bar{T}_1)}{\partial \bar{x}_i\, \partial \bar{x}_i} = \frac{\partial^2(\bar{p}_1, \bar{\rho}_1, \bar{T}_1)}{\partial t^2} \tag{17}$$

and

$$\frac{\partial \bar{q}_{i1}}{\partial \bar{t}} = - \frac{1}{\gamma}\frac{\partial \bar{p}_1}{\partial \bar{x}_i} \tag{18}$$

2.2 Porous Sheet Equations

A form for a set of equations which relate pressure, velocity, and temperature (or density) on opposite sides of the thin porous sheet is suggested by the integral form of the laws of mechanics. The integral mass, momentum, and energy equations may be written in terms of the dimensionless variables in equations 2.1(5) as

$$\int_{\bar{R}} \frac{\partial \bar{\rho}}{\partial \bar{t}}\, d\bar{V} + \int_{\bar{S}} \bar{\rho} n_i \bar{q}_i d\bar{S} = 0 \tag{1}$$

$$\int_{\bar{R}} \frac{\partial(\bar{\rho}\bar{q}_i)}{\partial \bar{t}}\, d\bar{V} + \int_{\bar{S}} \left\{ n_j \bar{\rho}\bar{q}_i \bar{q}_j + \frac{p_o n_i}{\rho_o\left(\frac{\omega}{\kappa}\right)^2} \bar{p} + \frac{\kappa\mu}{\rho_o\left(\frac{\omega}{\kappa}\right)} \left[\frac{2}{3} n_i \bar{q}_{k,k} - n_j(\bar{q}_{i,j} + \bar{q}_{j,1}) \right] \right\} d\bar{S} = 0 \tag{2}$$

and

$$\int_{\bar{R}} \frac{\partial}{\partial \bar{t}} \left[\bar{\rho}\left(\frac{\bar{q}^2}{2} + \bar{C}_v \bar{T} \right) \right] d\bar{V} + \int_{\bar{S}} n_i \bar{q}_i \left\{ \bar{\rho}\left(\frac{\bar{q}^2}{2} + \bar{C}_v \bar{T} \right) + \frac{p_o}{\rho_o\left(\frac{\omega}{\kappa}\right)^2} \bar{p} \right\} d\bar{S}$$

$$= \int_{\bar{S}} \left\{ \frac{\mu\kappa}{\rho_o\left(\frac{\omega}{\kappa}\right)} \left[\frac{2}{3} \bar{q}_{k,k} n_i \bar{q}_i + n_j(\bar{q}_{i,j} + \bar{q}_{j,i}) \bar{q}_i \right] + \frac{\kappa K T_o}{\rho_o\left(\frac{\omega}{\kappa}\right)^3} n_i \bar{T}_{,i} \right\} d\bar{S} \tag{3}$$

Consider a control volume which encloses the fluid flowing inside an element of the porous sheet, as shown in figure 1. The dimensionless thickness of the sheet, $\bar{h}$ is much less than 1. The control volume is fixed with respect to the sheet, which may be moving with a velocity, V_i. Since the control volume encloses only the fluid, and not the solid, the surface integrals extend over the interior wetted surface of the solid, and over the faces of the element where

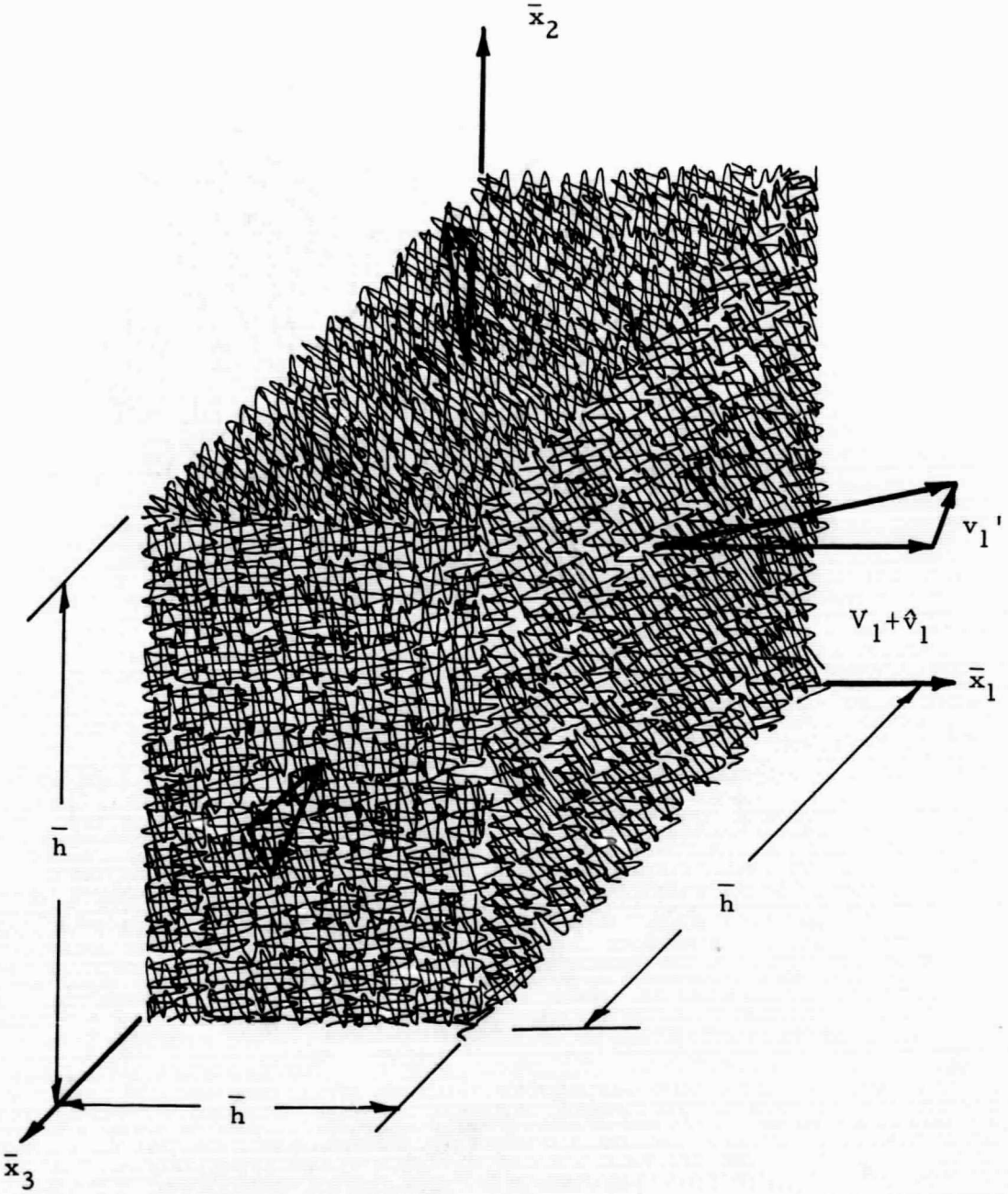

Figure 1.- Flow through porous element.

fluid is passing through. The velocity of the fluid may be expressed in terms of a relative velocity as

$$\bar{q}_i = V_i + v_i \tag{4}$$

Since the flow parameters will vary greatly from point to point within the porous element, they will be broken into average (over an area) and fluctuating parts. The average of a quantity is defined as

$$\hat{Q} = \frac{1}{A}\int Q \, dA \tag{5}$$

where A is an area whose size is small compared to a characteristic length of the problem, but large enough to give a meaningful average.

The fluctuation of a quantity is then

$$Q' = Q - \hat{Q} \tag{6}$$

In this problem the integrals will be taken over the faces of the control volume shown in figure 1.

The volume integrals in equations (1), (2), and (3) give time rates-of-change of mass and momentum and energy stored inside the control volume. These integrals and the surface integrals on the right side of the equations cannot be evaluated analytically. About all that can be said is that they are of two types: One with a time derivative, and one without.

The surface integral in equation (1) may be written as

$$\int_{\bar{S}} \bar{\rho} n_i \bar{q}_i \, d\bar{S} = \int_{S_{int}} \bar{\rho} n_i V_i \, d\bar{S} + h^{-2}\left\{\left[\hat{\rho}(V_1 + \hat{v}_1) + (\widehat{\rho' V_1'})\right]_{\bar{h}} - \left[\hat{\rho}(V_1 + \hat{v}_1) + (\widehat{\rho' V_1'}\right]_o\right\}$$

$$+ \text{ similar terms for faces 2 and 3 of element} \tag{7}$$

Consequently, the mass equation can be represented by the form

$$\Delta\left[\hat{\rho}(V_1 + \hat{v}_1)\right] = \bar{h}\left\{\frac{\partial}{\partial \bar{x}_2}\left[\hat{\rho}(V_2 + \hat{v}_2)\right] + \frac{\partial}{\partial \bar{x}_3}\left[\hat{\rho}(V_3 + \hat{v}_3)\right]\right\} + \frac{\partial M_1}{\partial t} + M_2 \tag{8}$$

where

$$\Delta\left[\hat{\rho}(V_1 + \hat{v}_1)\right] = \hat{\rho}(V_1 + \hat{v}_1)\Big|_o - \hat{\rho}(V_1 + \hat{v}_1)\Big|_{\bar{h}} \tag{9}$$

The first group of terms on the right of equation (8) represents flows in the plane of the sheet. The time derivative arises from the previously mentioned volume integral, and the last term, M_2, includes the integral over the internal wetted surface and terms like $(\widehat{\rho' v'})$. Similar forms are suggested for the momentum and energy equations, namely

$$\Delta\left[\hat{\rho}(V_1 + v_1)(V_i + v_i) + \delta_{1i}\frac{\hat{p}}{\bar{\gamma}}\right] = \frac{\partial L_{1i}}{\partial \bar{t}} + L_{2i}$$

$$+ \bar{h}\left\{\frac{\partial}{\partial \bar{x}_2}\left[\hat{\rho}(V_2 + \hat{v}_2)(V_i + \hat{v}_i) + \frac{\hat{p}}{\bar{\gamma}}\right] + \frac{\partial}{\partial \bar{x}_3}\left[\hat{\rho}(V_3 + \hat{v}_3)(V_i + \hat{v}_i) + \frac{\hat{p}}{\bar{\gamma}}\right]\right\} \tag{10}$$

and

$$\Delta\left[\hat{\rho}(V_1 + \hat{v}_1)\left(\frac{(V + \hat{v})^2}{2} + \bar{C}_v\hat{T}\right) + (V_1 + \hat{v}_1)\frac{\hat{p}}{\bar{\gamma}}\right] = \frac{\partial E_1}{\partial \bar{t}} + E_2$$

$$+ \bar{h}\left\{\frac{\partial}{\partial \bar{x}_2}\left[\hat{\rho}(V_2 + \hat{v}_2)\left(\frac{(V + \hat{v})^2}{2} + \bar{C}_v\hat{T}\right) + (V_2 + \hat{v}_2)\frac{\hat{p}}{\bar{\gamma}}\right]\right.$$

$$\left. + \frac{\partial}{\partial \bar{x}_3}\left[\rho(V_3 + \hat{v}_3)\left(\frac{(V + \hat{v})^2}{2} + \bar{C}_v\hat{T}\right) + (V_3 + \hat{v}_3)\frac{\hat{p}}{\bar{\gamma}}\right]\right\} \tag{11}$$

The functions M, L, and E must be evaluated experimentally in terms of the average flow parameters. Once this is done, equations (8), (10), and (11) give the necessary relations between flow parameters on either side of the porous sheet. Since the equations involve the velocity of the porous sheet, this quantity must either be specified or accounted for by adding appropriate equations for the motion of the sheet, such as plate or shell equations.

For the balance of this study, the porous sheet will be considered to be fixed. Cross-flow terms will be neglected since the sheet thickness is small.

With these conditions the sheet equations become

$$\Delta\left[\hat{\rho}\hat{v}\right] - \frac{\partial M_1}{\partial t} + M_2 \tag{12}$$

$$\Delta\left[\hat{\rho}\hat{v}_1\hat{v}_i + \delta_{1i}\frac{\hat{p}}{\gamma}\right] = \frac{\partial L_{1i}}{\partial t} + L_{2i} \tag{13}$$

and

$$\Delta\left[\hat{\rho}\hat{v}_1\left(\frac{\hat{v}^2}{2} + \bar{C}_v\hat{T}\right) + \hat{v}_1\frac{\hat{p}}{\gamma}\right] = \frac{\partial E_1}{\partial t} + E_2 \tag{14}$$

The average flow variables at each face of the porous sheet are assumed to equal the acoustic variables, that is

$$\hat{p} = \bar{p}, \tag{15a}$$

$$\hat{\rho} = \bar{\rho}, \tag{15b}$$

$$\hat{T} = \bar{T}, \tag{15c}$$

and

$$\hat{v}_i = \bar{q}_i \tag{15d}$$

Using these equations and the asymptotic expansions 2.1(12), equations (12), (13), and (14) become

$$\epsilon\, \Delta\left[\bar{q}_{11}\right] = \frac{\partial M_1}{\partial t} + M_2 + O(\epsilon^2) \tag{16}$$

$$\delta_{1i}\epsilon\, \Delta\left[\frac{\bar{p}_1}{\bar{\gamma}}\right] = \frac{\partial L_{1i}}{\partial t} + L_{2i} + O(\epsilon^2) \tag{17}$$

$$\epsilon^2\, \Delta\left[\bar{C}_v\bar{T}_1\bar{q}_{11} + \bar{q}_{11}\frac{\bar{p}_1}{\bar{\gamma}}\right] = \frac{\partial E_1}{\partial t} + E_2 + O(\epsilon^3) \tag{18}$$

A limited amount of experimental work (ref. 25) indicates that M_1 and M_2 are of order ϵ^2. The energy terms can only be of order ϵ^2 and, since the left side of (17) has the δ_{1i} factor L_{11} and L_{21} must be of order ϵ, while L_{12}, L_{13}, L_{22}, and L_{23} are of order ϵ^2. L_{11} was found to be proportional to $\dot{q}_{11}$, and L_{21} is a function of Mach number with a slight dependence on Reynolds number which can be relegated to the second order spot. Consequently, for acoustics problems involving thin porous sheets of material, the boundary conditions at the material become

$$\Delta\left[\bar{q}_{11}\right] = 0 \tag{19}$$

$$\epsilon\, \Delta\left[\bar{p}_1\right] = \epsilon\bar{m}\,\frac{\partial\bar{q}_{11}}{\partial t} + \Delta\bar{P}\left[\epsilon\bar{q}_{11}\right] \tag{20}$$

Here, $\bar{m}$ is a constant and $\Delta\bar{P}$ is a nonlinear function.

III. ONE-DIMENSIONAL PROBLEM

3.1 Pressure Drop Function

Little has been said to this point about the origin of the parameter ϵ. It could be associated with a forcing function, but in many acoustics problems, these do not appear explicitly. In this paper, it will be associated with a nominal sound pressure level.

The sound pressure level, or intensity, in decibels, is defined as

$$\mathrm{SPL} = 20\ \mathrm{Log}_{10}\left(\frac{p}{0.0002\ \mathrm{dynes/cm^2}}\right) \tag{1}$$

In terms of the dimensionless pressure, this becomes

$$\mathrm{SPL} = 20\ \mathrm{Log}_{10}\left(\frac{\epsilon\bar{\gamma}p_o\bar{p}_1}{0.0002\ \mathrm{dynes/cm^2}}\right) \tag{2}$$

or

$$\mathrm{SPL} = 20\ \mathrm{Log}_{10}(10^{10}\ \epsilon\bar{p}_1) - 3.0 \tag{3}$$

In order to make the dimensionless pressure vary from 0 to 1, ϵ may be chosen as some convenient power of 10 to give the correct SPL range. Table I shows the correspondence between SPL and ϵ when the dimensionless pressure is one.

The nonlinear pressure drop function in equation 2.2 (20) depends on ϵ. If that equation is divided by ϵ, all terms must be of order 1. The pressure drop term is $\frac{\Delta p\left[\epsilon q_{11}\right]}{\epsilon}$. Figure 2 shows a typical plot of this function for several values of ϵ. Each curve shown may be

TABLE I.- CORRESPONDENCE OF FLUCTUATION MAGNITUDE TO SOUND PRESSURE LEVEL

SPL, dB	ϵ
-3	10^{-10}
17	10^{-9}
37	10^{-8}
57	10^{-7}
77	10^{-6}
97	10^{-5}
117	10^{-4}
137	10^{-3}
157	10^{-2}
177	10^{-1}
197	1

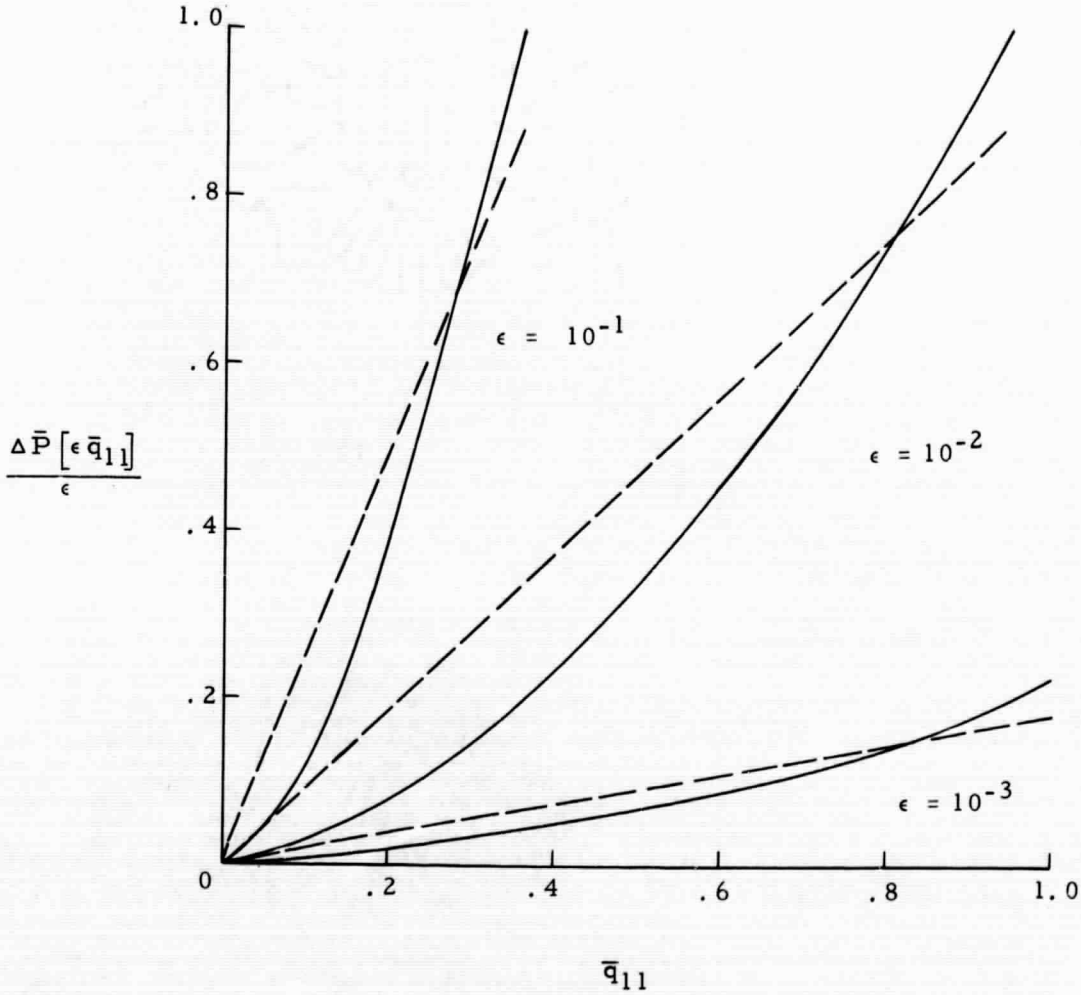

Figure 2.- Pressure drop functions for typical material.

approximated fairly well by a straight line. This does not mean that the nonlinearity is small. The slopes of the approximating lines in figure 2 vary from about 0.2 to 3.0 so, if this slope is thought of as an effective acoustic resistance, it must be concluded that the variation in resistance is large. Nevertheless, the fact that some straight line approximation is possible may permit perturbation methods to be used.

3.2 General Equations for Two Coupled Regions

In equations 2.1((17) and (18)) and 2.2 ((19) and (20)), let

$$U = \bar{q}_{11}, \tag{1a}$$

$$p = \frac{\bar{p}_1}{\gamma}$$

$$\frac{\bar{m}}{\gamma} = \rho_A, \tag{1c}$$

and

$$\Delta P = \frac{\Delta \bar{P}}{\gamma} \tag{1d}$$

The one-dimensional wave equation is then satisfied by

$$U = \sum_{n=-\infty}^{\infty} (u_n e^{-inx} + v_n e^{inx}) e^{int} \tag{2}$$

$$p = \sum_{n=-\infty}^{\infty} (u_n e^{-inx} - v_n e^{inx}) e^{int} \tag{3}$$

In equations (2) and (3), u_n and v_n are complex constants with

$$u_n = (\overline{u_{-n}}) \tag{4a}$$

$$v_n = (\overline{v_{-n}}) \tag{4b}$$

Each term with coefficient u_n represents a right-moving harmonic wave, while the v_n terms give left-moving waves.

Consider the two regions shown in figure 3. In each region there may be a periodic solution which is given by equations (2) and (3). At the sheet, there are the conditions

$$U_1 = U_2 \tag{5}$$

$$p_1 - p_2 = \rho_A \frac{\partial U}{\partial t} + \frac{\Delta p[\epsilon U]}{\epsilon} \tag{6}$$

and at the extreme ends of the regions there are general impedance-type boundary conditions

$$p_{1n} = Z_{1n}U_{1n} + P_{1n} \tag{7a}$$

$$p_{2n} = Z_{2n}U_{2n} + P_{2n} \tag{7b}$$

Here the subscripts 1 and 2 indicate the region while the subscript n indicates the harmonic.

If equations (2) and (3) are substituted into (5) through (7) and use is made of the orthogonality of complex exponentials, there results

$$u_{1n}e^{-inx_1} - v_{1n}e^{inx_1} = Z_{1n}\left[u_{1n}e^{-inx_1} + v_{1n}e^{inx_1}\right] + P_{1n} \tag{8a}$$

$$u_{1n} + v_{1n} = u_{2n} + v_{2n} \tag{8b}$$

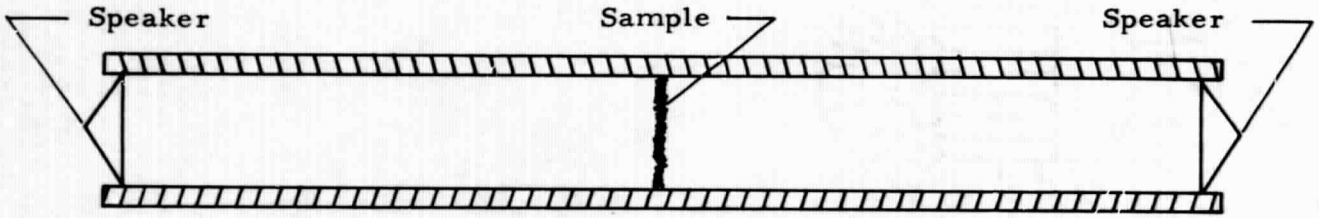

$$U_1(t)=U_2(t)$$

$$P_{1n}=Z_{1n}U_{1n}+P_{1n} \qquad P_1(t)-P_2(t)=\frac{\Delta P}{\epsilon}\left[\epsilon\, U(t)\right]+\rho A\frac{\partial U(t)}{\partial t} \qquad P_{2n}=Z_{2n}U_{2n}+P_{2n}$$

Figure 3.- One-dimensional problem for two regions coupled through a nonlinear porous sheet.

$$(u_{1n} - v_{1n}) - (u_{2n} - v_{2n}) = \frac{1}{2\pi}\int_{-\pi}^{\pi} e^{-int}\,\frac{\Delta P}{\epsilon}\left\{\epsilon\sum_{m=-\infty}^{\infty}(u_{1m} + v_{1m})e^{imt}\right\}dt$$

$$+ in\rho_A(u_{1n} + v_{1n}) \tag{8c}$$

$$u_{2n}e^{-inx_2} - v_{2n}e^{inx_2} = Z_{2n}\left[u_{2n}e^{-inx_2} + v_{2n}e^{inx_2}\right] + P_{2n} \tag{8d}$$

3.3 Approximate Methods of Solution

The above equations are an infinite set of nonlinear algebraic equations. They may be specialized to simulate a variety of situations. For example, if $P_{2n} = 0$, and $Z_{2n} = 1$, the region 2 will contain only right-moving waves. This simulates an infinite region where no waves are reflected. If Z_{2n} is infinite at $x_2 = \pi/2$, a rigid wall is simulated. The solution to these equations may be approximated in a variety of ways.

They are difficult to work with numerically, however, because in any iteration process, the integral term must be evaluated a large number of times as the iteration proceeds. In spite of this, the following technique has been successfully used to obtain numerical solutions.

3.3.1 Steepest Descent Iteration (ref. 43)

If an initial estimate for the solution is made, that is, $\tilde{u}_{1n}$, $\tilde{v}_{1n}$, $\tilde{u}_{2n}$, and $\tilde{v}_{2n}$ are specified, then equations 3.2 (8) may be used to compute the nonhomogeneous terms, P_{1n}, P_{2n}. The problem solution is then given by the minimum of the function

$$S = \sum_{n=-\infty}^{\infty}\left(|\tilde{P}_{1n} - P_{1n}|^2 + |\tilde{P}_{2n} - P_{2n}|^2\right) \tag{1}$$

A steepest descent technique was used for locating the minimum of equation (20). This method amounts to following the gradient of the potential function, S, during the iteration. The reader interested in further details of the method may find them in reference 43.

3.3.2 Collocation Method

The integral which causes numerical difficulty may be eliminated by adopting a different criterion (ref. 44) for satisfying the pressure drop condition.

For brevity, we introduce the notations

$$V_n = u_{1n} + v_{1n} = u_{2n} + v_{2n} \tag{1}$$

and

$$\Delta p_n = \frac{1}{2\pi} \int_{-\pi}^{\pi} e^{-int} \frac{\Delta P}{\epsilon} \left\{ \epsilon \sum_{m=-\infty}^{\infty} V_m e^{imt} \right\} dt \tag{2}$$

In terms of these variables, equations 3.2 (8) become

$$\Delta p_n = Z_n V_n + P_n \tag{3}$$

where

$$Z_n = \left[\frac{Z_{1n} \cos(nx_1) + i \sin(nx_1)}{\cos(nx_1) + iZ_{1n} \sin(nx_1)} - \frac{Z_{2n} \cos(nx_2) + i \sin(nx_2)}{\cos(nx_2) + iZ_{2n} \sin(nx_2)} \right] - in\rho_A \tag{4}$$

and

$$P_n = \left[\frac{P_{1n}}{\cos(nx_1) + iZ_{1n}\sin(nx_1)} - \frac{P_{2n}}{\cos(nx_2) + iZ_{2n}\sin(nx_2)} \right] \tag{5}$$

In equation (3), the Δp_n are the complex Fourier coefficients of the steady flow pressure drop, Δp. Note that the inertia term from equation 2.2 (20) is included on the right of equation (3). To satisfy the pressure drop law continuously would require that

$$\Delta p(t) = \frac{\Delta P\{\epsilon V(t)\}}{\epsilon} \tag{6}$$

An approximation to the condition (6) is to use a least-squares criterion at discrete points in time, that is, use the minimum of the function

$$S = \sum_{n=0}^{N-1} \left\{ \Delta p(t_n) - \frac{\Delta P\{\epsilon V(t_n)\}}{\epsilon} \right\}^2 \tag{7}$$

to approximate the problem solution.

The instantaneous pressure and velocity are given in terms of their Fourier coefficients by

$$\Delta p(t) = \sum_{k=-L}^{L} \Delta p_k e^{ikt}, \qquad V(t) = \sum_{k=-L}^{L} V_k e^{ikt} \tag{8), (9}$$

where

$$0 < L < \frac{N}{2}$$

Evenly spaced intervals are taken in (7), so that

$$t_n = \frac{2\pi m}{N} \tag{10}$$

so that the potential function, S becomes

$$S = \sum_{n=0}^{N-1} \left\{ \sum_{k=-L}^{L} (Z_k V_k + P_k) e^{\frac{2\pi i k n}{N}} - \frac{\Delta P \left\{ \epsilon \sum_{K=-L}^{L} V_k e^{\frac{2\pi i k n}{N}} \right\}}{\epsilon} \right\} \tag{11}$$

A powerful computational algorithm, known as the Fast Fourier Transform, has been developed for working with the sums which appear inside equation (11). Details of this are available in references 45 through 48.

Simeonov's method (ref. 53) or the steepest descent procedure could be used to minimize the function given in equation (11) with respect to the Fourier coefficients, V_n. When this is done, however, a summation, which is analogous to the integral in equation 3.2 (8c), must be made repeatedly during the iteration process. This may be avoided by using equation (6) to solve for the velocity at N discrete points in time, t_n.

The inversion of equation (9) gives

$$V_n = \frac{1}{N} \sum_{m=0}^{N-1} V(t_m) e^{-\frac{2\pi i n m}{N}} \tag{12}$$

Using this result with equations (3), (6), and (8) gives

$$\sum_{m=1}^{N-1} G_{nm}V(t_m) + P(t_n) = \frac{\Delta P\left\{\epsilon V(t_n)\right\}}{\epsilon} \tag{13}$$

where

$$G_{nm} = \frac{1}{N}\sum_{k=-L}^{L} Z_k e^{\frac{2\pi ik(n-m)}{N}} \tag{14}$$

and

$$P(t_n) = \sum_{k=-L}^{L} P_n e^{\frac{2\pi ikn}{N}} \tag{15}$$

The solution of the nonlinear algebraic equations (13) satisfies (6) at a finite set of times. To satisfy the pressure drop relation continuously would require an infinite set of equations. The advantage of (13) is that the transform of the nonlinear function does not appear. A variety of techniques may be used to solve (13). Since it gives the minimum of (7), which is zero, the steepest descent procedure, or Simeonov's method of descent could be used, or a technique of successive approximations might be a feasible method of solution. A disadvantage of this set of equations is the need to invert the array G_{nm}, which may be a very large order matrix.

3.3.3 Linearized Perturbation Equations

The data shown in figure 2 indicate that the pressure drop function may be written as

$$\frac{\Delta P\left[\epsilon \bar{q}_{11}\right]}{\epsilon} = R\bar{q}_{11} + \delta\Gamma\left[\bar{q}_{11}\right] \tag{1}$$

R, Γ, and δ each depend on the parameter ϵ. For purposes of analysis, δ is taken to be a small parameter which is large when compared to ϵ but small compared to one.

$$\delta = << 1 \tag{2a}$$

$$R = O(1) \tag{2b}$$

$$\Gamma\left[\bar{q}_{11}\right] = O(1) \tag{2c}$$

Using equations 3.2 (8) again, and assuming a power series solution in terms of the parameter δ,

$$u_{1n} \sim u_{1n}^{(0)} + \delta u_{1n}^{(1)} + \ldots \tag{3a}$$

$$v_{1n} \sim v_{1n}^{(0)} + \delta v_{1n}^{(1)} + \ldots \tag{3b}$$

$$u_{2n} \sim u_{2n}^{(0)} + \delta u_{2n}^{(1)} + \ldots \tag{3c}$$

and

$$v_{2n} \sim v_{2n}^{(0)} + \delta v_{2n}^{(1)} + \ldots \tag{3d}$$

gives the zeroth and first-order linear power series equations

$$u_{1n}^{(0)}e^{-inx_1} - v_{1n}e^{inx_1} = Z_{1n}\left[u_{1n}^{(0)}e^{-inx_1} + v_{1n}^{(0)}e^{inx_1}\right] + P_{1n} \tag{4a}$$

$$u_{1n}^{(0)} + v_{1n}^{(0)} = u_{2n}^{(0)} + v_{2n}^{(0)} \tag{4b}$$

$$(u_{1n}^{(0)} - v_{1n}^{(0)}) - (u_{2n}^{(0)} - v_{2n}^{(0)}) = (R + in\rho_A)(u_{1n}^{(0)} + v_{1n}^{(0)}) \tag{4c}$$

$$u_{2n}^{(0)}e^{-inx_2} - v_{2n}^{(0)}e^{inx_2} = Z_{2n}\left[u_{2n}^{(0)}e^{-inx_2} + v_{2n}^{(0)}e^{inx_2}\right] + P_{2n} \tag{4d}$$

$$u_{1n}^{(1)}e^{-inx_1} - v_{1n}^{(1)}e^{inx_1} = Z_{1n}\left[u_{1n}^{(1)}e^{-inx_1} + v_{1n}^{(1)}e^{inx_1}\right] \tag{5a}$$

$$u_{1n}^{(1)} + v_{1n}^{(1)} = u_{2n}^{(1)} + v_{2n}^{(1)} \tag{5b}$$

$$(u_{1n}^{(1)} - v_{1n}^{(1)}) - (u_{2n}^{(1)} - v_{2n}^{(1)}) = (R + in\rho_A)(u_{1n}^{(1)} + v_{1n}^{(1)}) + \frac{1}{2\pi}\int_{-\pi}^{\pi} e^{-int}\Gamma\left[V^{(0)}(t)\right] dt \tag{5c}$$

$$u_{2n}^{(1)}e^{-inx_2} - v_{2n}^{(1)}e^{inx_2} = Z_{2n}\left[u_{2n}^{(1)}e^{-inx_2} + v_{2n}^{(1)}e^{inx_2}\right] \tag{5d}$$

The advantage in this approach is apparent. Solving each set of linear equations is a trivial matter. The integral term which causes computational difficulty in an iteration scheme must be evaluated only once to obtain the nonhomogeneous part of the first-order equations. There is a danger in using this method in that the choice of ϵ will not give a solution such that $\bar{q}_{11}$ varies as expected. For example, in figure 2, when $\epsilon = 10^{-2}$ it is assumed that $\bar{q}_{11}$ will have a maximum value of 1.0. When $\epsilon = 10^{-1}$, $(\bar{q}_{11})_{max}$ should be about 0.4. It is possible to extend this reasoning to obtain an iteration scheme based on power series equations.

3.4 Exact Solutions

In terms of the notation introduced in equation 3.2 (1), the one-dimensional wave equation is

$$\frac{\partial^2 U}{\partial t^2} = \frac{\partial^2 U}{\partial x^2} \tag{1}$$

and

$$\frac{\partial U}{\partial t} = - \frac{\partial p}{\partial x} \tag{2}$$

The classical solution (ref. 49) to (43) is

$$U = f(t - x) + g(t + x) \tag{3}$$

Figure 4a depicts a problem where an incident wave, f_1, is reflected from a porous sheet which is backed up by a perfect absorber. At the porous sheet, we use a special case of the pressure drop law, with $\rho_A = 0$.

$$p_1 - p_2 = \frac{\Delta P\left[\epsilon U\right]}{\epsilon} \tag{4}$$

The acoustic velocity is continuous at the sample and there is only a right moving wave behind the sample.

$$f_1(t) + g_1(t) - f_2(t) = 0 \tag{5}$$

$$f_1(t) - g_1(t) - f_2(t) = \frac{\Delta P\left[\epsilon(f_1(t) + g_1(t))\right]}{\epsilon} \tag{6}$$

Let

$$\beta_2(U) = \frac{\Delta P\left[\epsilon U\right]}{\epsilon} + 2U, \tag{7}$$

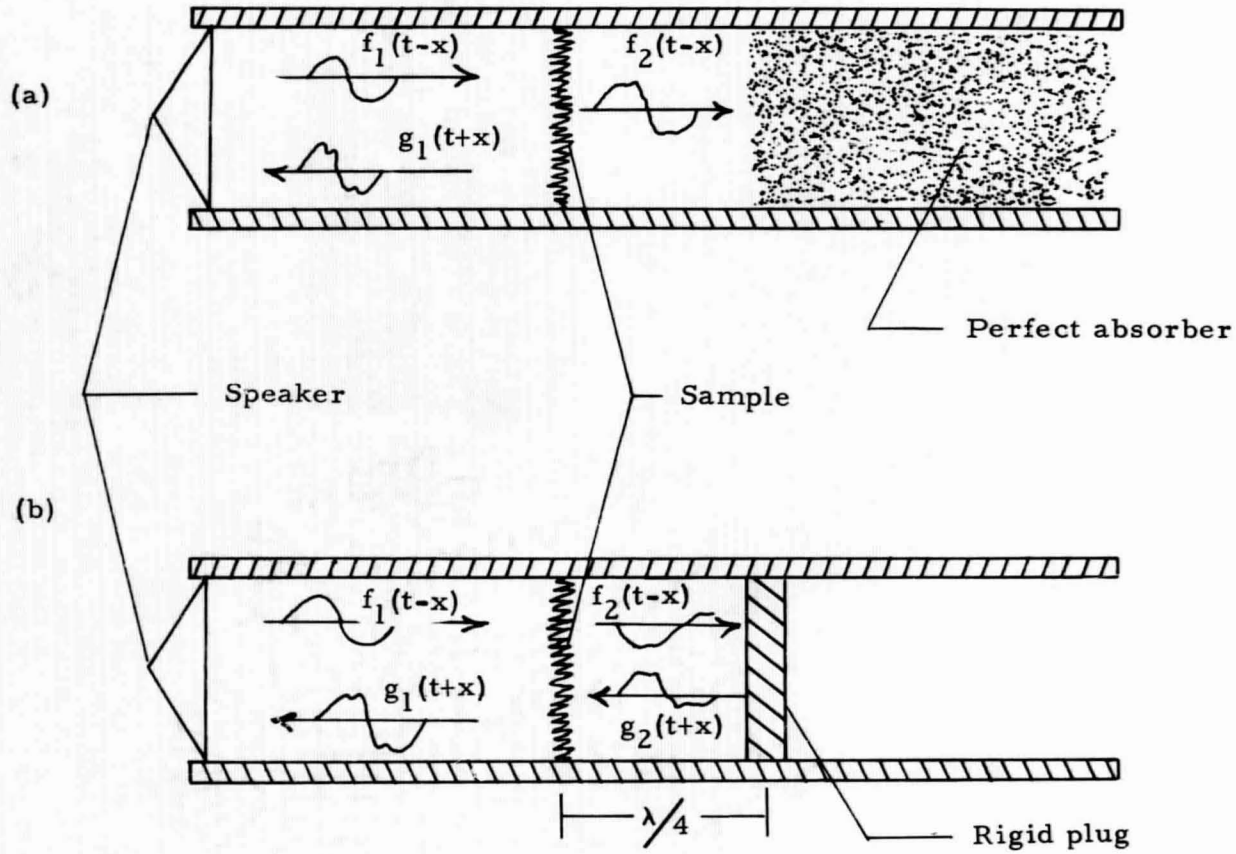

Figure 4.- Waves reflected from a porous sheet with nonlinear resistance.

then, by subtracting (5) from (6) and adding $2f_1(t)$ to each side of the resulting equation, it may be shown that

$$\beta_2(f_1(t) + g_1(t)) = 2f_1(t) \tag{8}$$

$$g_1(t) = - f_1(t) + \beta_2^{-1}(2f_1(t)) \tag{9}$$

The exact solution, given by equation (9), depends on the possibility of inverting the function $\beta_2(U)$. This presents no practical difficulty. Since $\frac{\Delta P[\epsilon U]}{\epsilon}$ must be constructed from experimental data, there can be no loss in accuracy by directly constructing the inverse function, β_2^{-1}, from the same data.

For the problem depicted in figure 4b, the equations which govern the transmitted and reflected waves are

$$f_1(t) + g_1(t) - f_2(t) - g_2(t) = 0 \tag{10}$$

$$f_2(t - w) + g_2(t + w) = 0 \tag{11}$$

$$f_1(t) - g_1(t) - f_2(t) + g_2(t) = \frac{\Delta P[\epsilon(f_1(t) + g_1(t))]}{\epsilon} \tag{12}$$

The incident wave, f, is considered to be given. Equations (10), (11), and (12) may be used to eliminate f_2 and g_2 to give an equation for g_1. First adding and then subtracting equations (10) and (12) gives

$$f_2(t) = f_1(t) - \frac{1}{2}\frac{\Delta P[\epsilon(f_1(t) + g_1(t))]}{\epsilon} \tag{13}$$

$$g_2(t) = g_1(t) + \frac{1}{2}\frac{\Delta P[\epsilon(f_1(t) + g_1(t))]}{\epsilon} \tag{14}$$

Substituting these equations into (11) gives

$$f_1(t - w) + g_1(t + w) - \frac{1}{2}\frac{\Delta P\left[\epsilon(f_1(t - w) + g_1(t - w))\right]}{\epsilon}$$

$$+ \frac{1}{2}\frac{\Delta P\left[\epsilon(f_1(t + w) + g_1(t + w))\right]}{\epsilon} = 0 \qquad (15)$$

Since (15) holds for all values of t, it must hold at $t - w$ and $t + w$, thus

$$f_1(t) + g_1(t + 2w) - \frac{1}{2}\frac{\Delta P\left[\epsilon(f_1(t) + g_1(t))\right]}{\epsilon}$$

$$+ \frac{1}{2}\frac{\Delta P\left[\epsilon(f_1(t + 2w) + g_1(t + 2w))\right]}{\epsilon} = 0 \qquad (16)$$

$$f_1(t - 2w) + g_1(t) - \frac{1}{2}\frac{\Delta P\left[\epsilon(f_1(t - 2w) + g_1(t - 2w))\right]}{\epsilon}$$

$$+ \frac{1}{2}\frac{\Delta P\left[\epsilon(f_1(t) + g_1(t))\right]}{\epsilon} = 0 \qquad (17)$$

Adding (16) and (17) gives the identity

$$f_1(t) + g_1(t) + f_1(t - 2w) + g_1(t + 2w) = 0 \qquad (18)$$

Let $f_1(t)$ have a period equal to $4w$, then

$$f_1(t) + g_1(t) = -(f_1(t + 2w) + g_1(t + 2w)) \qquad (19)$$

Now, if $\frac{\Delta P\left[\epsilon U\right]}{\epsilon}$ is odd, then substituting (19) into (16) gives

$$f_1(t) + g_1(t + 2w) = \frac{\Delta P\left[\epsilon(f_1(t) + g_1(t))\right]}{\epsilon} \tag{20}$$

Letting t go to $t - 2w$ in (19) and substituting into (17) gives

$$f_1(t + 2w) + g_1(t) = - \frac{\Delta P\left[\epsilon(f_1(t) + g_1(t))\right]}{\epsilon} \tag{21}$$

Adding and subtracting $f_1(t)$ in (21) gives

$$\frac{\Delta P\left[\epsilon(f_1(t) + g_1(t))\right]}{\epsilon} + (f_1(t) + g_1(t)) = f_1(t) - f_1(t + 2w) \tag{22}$$

Now, if

$$\beta_1(U) = \frac{\Delta P\left[\epsilon U\right]}{\epsilon} + U \tag{23}$$

the exact solution for the reflected wave is

$$g_1(t) = - f_1(t) + \beta_1^{-1}\left[f_1(t) - f_1(t + 2w)\right] \tag{24}$$

In the general case, where the backing is not a perfect absorber, or where the rigid wall is not exactly 1/4 wavelengths away, the waves behind the sample are related by the convolution integral

$$g_2(t) = \int_{-\pi}^{\pi} G\,(t - \tau) f_2(\tau) d\tau = G * f_2 \tag{25}$$

where

$$G(t - \tau) = \frac{1}{2\pi} \sum_{n=-\infty}^{\infty} \left(\frac{1 - Z_n(0)}{1 + Z_n(0)}\right) e^{in(t-\tau)} \tag{26}$$

and $Z_n(0)$ is the acoustic impedance in the backing cavity, evaluated at the sample. Thus, in general, the problems of wave reflection from a porous absorber with nonlinear resistance depends on the solution of the set of nonlinear functional equations (10), (12), and (25). No general theory exists for the solution of functional equations, although a number of examples are discussed in the book by Aczel (ref. 50). A numerical approach to their solution gives equations like 3.3.2 (13), that is, large sets of nonlinear algebraic equations.

IV. SCATTERING FROM A POROUS ELLIPTICAL CYLINDER

4.1. Coordinates, Governing Equations, and Boundary Conditions

Figure 5 shows the elliptical cylinder coordinates which will be used in this section. These coordinates are define by

$$x = h \cosh \xi \cos \eta \tag{1}$$

$$y = h \sinh \xi \sin \eta \tag{2}$$

As shown in figure 5, curves with ξ = constant are ellipses with focal points at $x = \pm h$. Curves where η = constant give hyperbolas with focal points which correspond to those of the ellipses.

Let $\overline{q}_{11} = n_i q_i$ and denote a unit normal to the elliptical cylinder by n_i. Then the governing equations are

$$\frac{\partial^2 p}{\partial x_i \, \partial x_i} = \frac{\partial^2 p}{\partial t^2} \tag{3}$$

$$\frac{\partial q_i}{\partial t} = - \frac{\partial p}{\partial x_i} \tag{4}$$

$$\Delta\left[n_i q_i\right] = 0 \tag{5}$$

$$\Delta\left[p\right] = \rho_A \frac{\partial(n_i q_i)}{\partial t} + \frac{\Delta P\left[\epsilon n_i q_i\right]}{\epsilon} \tag{6}$$

When these conditions are expressed in elliptical coordinates, they become

$$\frac{\partial^2 p}{\partial \xi^2} + \frac{\partial^2 p}{\partial \eta^2} = 2k^2(\cosh 2\xi - \cos 2\eta)\frac{\partial^2 p}{\partial t^2} \tag{7}$$

$$\frac{\partial q_\xi}{\partial t} = \frac{-1}{\sqrt{2k^2(\cosh 2\xi - \cos 2\eta)}} \frac{\partial p}{\partial \xi} \tag{8}$$

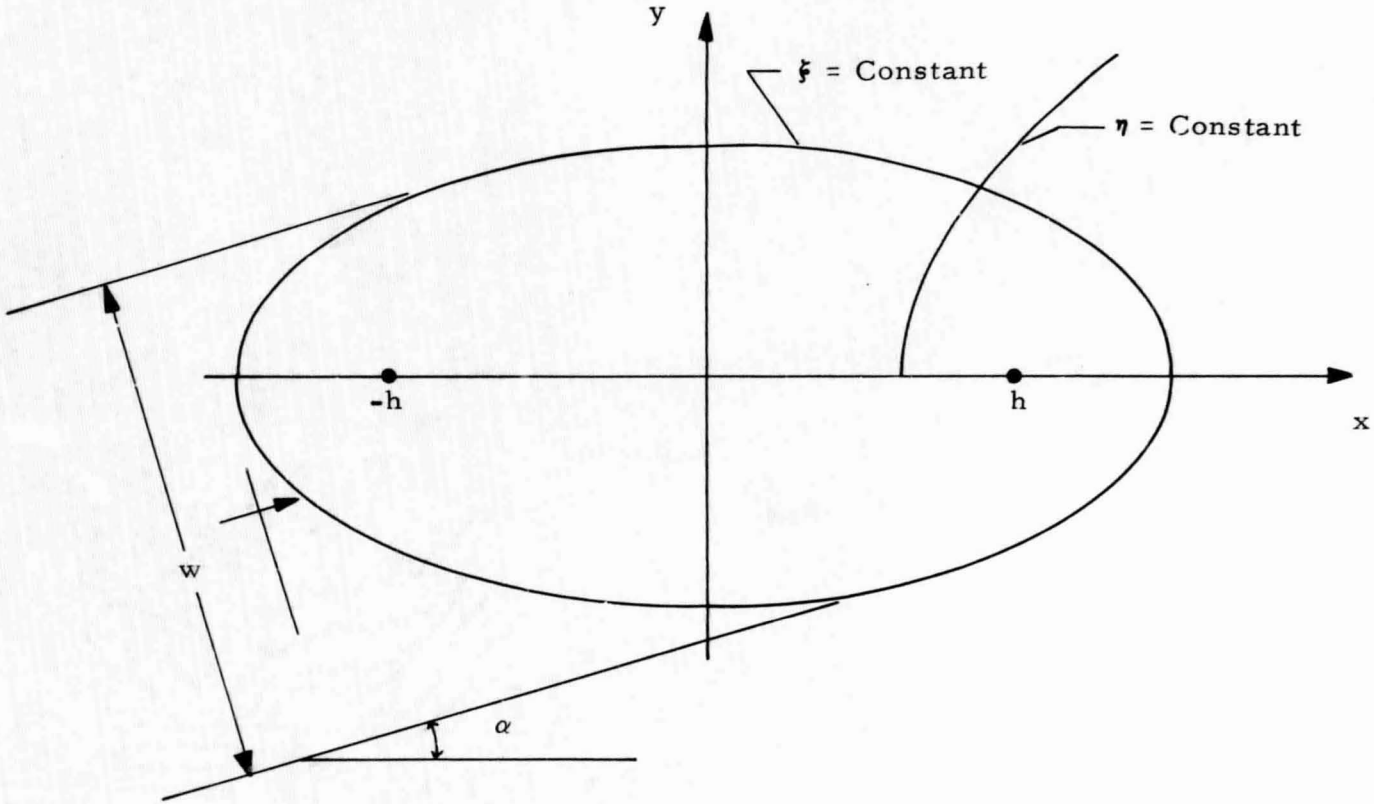

Figure 5.- Elliptical coordinates.

$$\frac{\partial q_\eta}{\partial \xi} = \frac{-1}{\sqrt{2k^2(\cosh 2\xi - \cos 2\eta)}} \frac{\partial p}{\partial \eta} \tag{9}$$

$$\Delta\left[q_\xi\right] = 0 \tag{10}$$

$$\Delta\left[p\right] = \rho_A \frac{\partial q_\xi}{\partial t} + \frac{\Delta p\left[\epsilon q_\xi\right]}{\epsilon} \tag{11}$$

Here, q_ξ is the velocity along a curve η = constant, ξ_o denotes the surface of the porous cylinder, and

$$k = \frac{h}{2} \tag{12}$$

4.2. Derivation of Solutions to Mathieu's Equation

We seek a periodic solution to equation 4.1(7) of the form

$$p(\xi,\eta,t) = \sum_{n=-\infty}^{\infty} p_n(\xi,\eta)\, e^{int} \tag{1}$$

For these solutions the wave equation becomes

$$\frac{\partial^2 p_n}{\partial \eta^2} + \frac{\partial^2 p_n}{\partial \eta^2} + (nh)^2(\cosh^2 \xi - \cos^2 \eta)p_n(\xi,\eta) = 0 \tag{2}$$

and the velocity is related to the pressure by

$$q_\xi = \frac{-1}{\sqrt{2k^2(\cosh 2\xi - \cos 2\eta)}} \sum_{n=-\infty}^{\infty} \frac{\partial p_n}{\partial \xi} \frac{e^{int}}{in} \tag{3}$$

$$q_\eta = \frac{-1}{\sqrt{2k^2(\cosh 2\xi - \cos 2\eta)}} \sum_{n=-\infty}^{\infty} \frac{\partial p_n}{\partial \eta} \frac{e^{int}}{in} \tag{4}$$

The singular terms in equations (3) and (4) require that $p_o(\xi,\eta)$ = constant. Although these terms add a small circulation and divergence to the flow field, they will be omitted for the remainder of this discussion.

Separable solutions of equation (2) are of the form

$$p_n(\xi,\eta) = \psi_n(\xi)\ \phi_n(\eta) \tag{5}$$

Inserting this form into the wave equation gives

$$\phi_n''(\eta) + (b - s_n \cos^2 \eta)\ \phi_n(\eta) = 0 \tag{6}$$

and

$$\psi_n''(\xi) - (b - s_n \cosh^2 \xi)\ \psi_n(\xi) = 0 \tag{7}$$

where

$$s_n = n^2h^2 \tag{8}$$

For the development of the theory of Mathieu functions, the notation of the National Bureau of Standards Tables, reference 42, will be used since later computations are to be based on these tables. The method of derivation is that which Arscott gives in his book (ref. 37).

4.2.1 Circumferential Fourier Series Solutions

In equations 4.2(6) and 4.2(7), which are called Mathieus equation and Mathieu's modified equation, b is a separation constant which depends on s_n. For $\phi_n(\eta)$ to be periodic, b will take a set of values. To each of these values, there corresponds an independent solution. These solutions form a complete orthogonal set.

Arscott has given a clear and rigorous proof that these solutions are of the form

$$Se_{2r}(s_n,\eta) = \sum_{k=0}^{\infty} De_{2k}^{(2r)} \cos 2k\eta\ ;\quad be_{2r}(s_n) \tag{1}$$

$$Se_{2r+1}(s_n,\eta) = \sum_{k=0}^{\infty} De_{2k+1}^{(2r+1)} \cos(2k+1)\eta \; ; \; be_{2r+1}(s_n) \tag{2}$$

$$So_{2r+1}(s_n,\eta) = \sum_{k=0}^{\infty} Do_{2k+1}^{(2r+1)} \sin(2k+1)\eta \; ; \; bo_{2r+1}(s_n) \tag{3}$$

$$So_{2r+2}(s_n,\eta) = \sum_{k=0}^{\infty} Do_{2k+2}^{(2r+2)} \sin(2k+2)\eta \; ; \; bo_{2r+2}(s_n) \tag{4}$$

In equation 4.2.1(4) we have deviated slightly from the NBS notation by using the subscript (2r + 2) instead of 2r. This allows the summation to extend from o to ∞ in all cases. Functions and coefficients with the same <u>numerical</u> value are still as defined in the NBS tables. Note that the even functions include the letter "e" in their symbols, and the odd functions use the letter "o." Methods of evaluating the coefficients De, Do, and separation constants, be, bo are given in the NBS tables. The coefficients are normalized according to the condition

$$Se_r(s_n,o) = 1 \tag{5}$$

$$\left.\frac{dSo_r}{d\eta}\right|_{\eta=o} = 1 \tag{6}$$

This normalization gives the orthogonality conditions

$$\int_o^{2\pi} Se_r(s_n,\eta)\; So_m(s_n,\eta)d\eta = 0 \tag{7}$$

$$\int_o^{2\pi} Se_r(s_n,\eta)\; Se_m(s_n,\eta)d\eta = \begin{cases} o, & m \neq r \\ N_r, & m = r \end{cases} \tag{8}$$

$$\int_o^{2\pi} So_r(s_n,\eta)\; So_m(s_n,\eta)d\eta = \begin{cases} o, & m \neq r \\ N_r', & m = r \end{cases} \tag{9}$$

4.2.2 Radial Bessel Function Product Solutions

To generate the radial solutions for the modified Mathieu equation, use may be made of the formula

$$\psi_n(\xi) = C_n \int_0^{2\pi} G_n(\xi,\eta)\ \phi_n(\eta)d\eta \tag{1}$$

It may be shown that the function given by equation (1) satisfies the modified Mathieu equation if $G_n(\xi,\eta)$ is any solution of the wave equation and $\phi_n(\eta)$ is any of the periodic solutions of Mathieu's equation.

Appropriate kernels for equation (1) are the cylindrical waves. To get these, the wave equation is transformed into polar coordinates where it is

$$\frac{1}{r}\frac{\partial}{\partial r}\left(r\ \frac{\partial G_n(r,\theta)}{\partial r}\right) + \frac{1}{r^2}\frac{\partial^2 G_n(r,\theta)}{\partial\theta^2} + n^2 G_n(r,\theta) = 0 \tag{2}$$

where

$$x = r\cos\theta \tag{3}$$

$$y = r\sin\theta \tag{4}$$

Equation (31) has the solutions

$$G_n(r,\theta) = H_\lambda^{(1,2)}(nr)\ \begin{matrix}\cos\\ \sin\end{matrix}\ \lambda\theta\ \ ;\ \lambda = 0,1,2,\ldots \tag{5}$$

In reference 51, Watson gives a proof of Graf's addition theorem for Bessel functions, which is

$$H_\lambda(\bar{\omega})\ \begin{matrix}\cos\\ \sin\end{matrix}\left\{\lambda\psi\right\} = \sum_{m=-\infty}^{\infty} H_{\lambda+m}(Z)J_m(z)\ \begin{matrix}\cos\\ \sin\end{matrix}\left\{m\phi\right\} \tag{6}$$

In this formula

$$\varpi = \sqrt{Z^2 + z^2 - 2Zz \cos \theta} \tag{7}$$

$$\varpi \cos \psi = Z - z \cos \theta \tag{8}$$

$$\varpi \sin \psi = z \sin \theta \tag{9}$$

If we let

$$\phi = 2\eta \tag{10}$$

$$Z = \frac{\sqrt{s_n}}{2} e^{\xi} \tag{11}$$

$$z = -\frac{\sqrt{s_n}}{2} e^{-\xi} \tag{12}$$

then

$$\varpi = nr \tag{13}$$

and

$$\cos \theta = \cos \eta \cos \psi - \sin \eta \sin \psi \tag{14}$$

$$\sin \theta = \sin \eta \sin \psi + \cos \eta \cos \psi \tag{15}$$

$$H_\lambda(nr) \begin{matrix}\cos\\ \sin\end{matrix}\{\lambda\psi\} = \sum_{m=-\infty}^{\infty} (-1)^m H_{\lambda+m}\left(\frac{\sqrt{s_n}}{2} e^{\xi}\right) J_m\left(\frac{\sqrt{s_n}}{2} e^{-\xi}\right) \begin{matrix}\cos\\ \sin\end{matrix}\{2m\eta\} \tag{16}$$

Equations (6) and (16) hold for Hankel functions of the first or the second kind.

Although any solution of the wave equation serves as a kernel for equation (1), it is possible to obtain trivial solutions.

Nontrivial solutions are found by selecting kernels which have the same period as the generating solution, ϕ_n, and which are even or odd as ϕ_n is even or odd.

Corresponding to each of the circumferential solutions, 4.2.1(1) through 4.2.1(4), there are the radial solutions

$$He_{2r}(s_n,\xi) = C_{2r}\int_0^{2\pi} H_0(nr)Se_{2r}(s_n,\eta)d\eta;\ be_{2r}(s_n) \tag{17}$$

$$He_{2r+1}(s_n,\xi) = C_{2r+1}\int_0^{2\pi} H_1(nr)\cos\theta\ Se_{2r+1}(s_n,\eta)d\eta;\ be_{2r+1}(s_n) \tag{18}$$

$$Ho_{2r+1}(s_n,\xi) = d_{2r+1}\int_0^{2\pi} H_1(nr)\sin\theta\ So_{2r+1}(s_n,\eta)d\eta;\ bo_{2r+1}(s_n) \tag{19}$$

$$Ho_{2r+2}(s_n,\xi) = d_{2r+2}\int_0^{2\pi} H_2(nr)\sin 2\theta\ So_{2r+2}(s_n,\eta)d\eta;\ bo_{2r+2}(s_n) \tag{20}$$

In these equations, Hankel functions of the first or second kinds may be used, so that the complex conjugates of these expressions are independent radial solutions. By using the trigonometric identities (14) and (15), Graf's addition theorem (16), and the expansions for the periodic Mathieu functions, the radial solutions are reduced to the series

$$He_{2r}(s_n,\xi) = \frac{(-1)^r}{De_0}\sqrt{\frac{\pi}{2}}\sum_{m=0}^{\infty}(-1)^m De_{2m}^{(2r)} H_m\left(\frac{\sqrt{s_n}}{2}e^{\xi}\right)J_m\left(\frac{\sqrt{s_n}}{2}e^{-\xi}\right);\ be_{2r}(s_n) \tag{21}$$

$$He_{2r+1}(s_n,\xi) = \frac{(-1)^r}{De_1}\sqrt{\frac{\pi}{2}}\sum_{m=0}^{\infty}(-1)^m De_{2m+1}^{(2r+1)}\left[H_{m+1}\left(\frac{\sqrt{s_n}}{2}e^{\xi}\right)J_m\left(\frac{\sqrt{s_n}}{2}e^{-\xi}\right)\right.$$

$$\left. + H_m\left(\frac{\sqrt{s_n}}{2}e^{\xi}\right)J_{m+1}\left(\frac{\sqrt{s_n}}{2}e^{-\xi}\right)\right];\ be_{2r+1}(s_n) \tag{22}$$

$$Ho_{2r+1}(s_n,\xi) = \frac{(-1)^r}{Do_1}\sqrt{\frac{\pi}{2}}\sum_{m=0}^{\infty}(-1)^m Do_{2m+1}^{(2r+1)}\left[H_{m+1}\left(\frac{\sqrt{s_n}}{2}e^{\xi}\right)J_m\left(\frac{\sqrt{s_n}}{2}e^{-\xi}\right)\right.$$

$$\left. - H_m\left(\frac{\sqrt{s_n}}{2}e^{\xi}\right)J_{m+1}\left(\frac{\sqrt{s_n}}{2}e^{-\xi}\right)\right];\ bo_{2r+1}(s_n) \tag{23}$$

$$Ho_{2r+2}(s_n,\xi) = \frac{(-1)^r}{Do_2}\sqrt{\frac{\pi}{2}}\sum_{m=0}^{\infty}(-1)^m Do_{2m+2}^{(2r+2)}\left[H_{m+2}\left(\frac{\sqrt{s_n}}{2}e^{\xi}\right)J_m\left(\frac{\sqrt{s_n}}{2}e^{-\xi}\right)\right.$$

$$\left. - H_m\left(\frac{\sqrt{s_n}}{2}e^{\xi}\right)J_{m+2}\left(\frac{\sqrt{s_n}}{2}e^{-\xi}\right)\right];\ bo_{2r+2}(s_n) \tag{24}$$

Equations (21) through (24) are the radial solution which will be used for later computations. Since the complex conjugates of those solutions are also solutions, these equations each give two independent radial solutions. To distinguish these we add superscripts such as $He_{2r}^{(1)}$, $He_{2r}^{(2)}$.

Asymptotic expansions for the radial solutions with large arguments may be found from the known expansions for Hankel functions. In reference 52, Hildebrand gives the formula

$$H_p^{(1,2)}(x) \sim \sqrt{\frac{2}{\pi x}}\, e^{\pm i\left[x - \frac{(2p+1)\pi}{4}\right]} \tag{25}$$

With this formula and the values of the Bessel function at the origin

$$J_p(o) = \begin{cases} 1, & p = 0 \\ 0, & p \neq 0 \end{cases} \tag{26}$$

the asymptotic formulae for radial solutions may be shown to be

$$He_{2r}^{(1,2)}(s_n,\xi) \sim \frac{(-1)^r}{\sqrt{\frac{\sqrt{s_n}}{2} e^{\xi}}} e^{\pm i\left[\frac{\sqrt{s_n}}{2} e^{\xi} - \frac{\pi}{4}\right]} \tag{27}$$

$$He_{2r+1}^{(1,2)}(s_n,\xi) = \frac{(-1)^r}{\sqrt{\frac{\sqrt{s_n}}{2} e^{\xi}}} e^{\pm i\left[\frac{\sqrt{s_n}}{2} e^{\xi} - \frac{3\pi}{4}\right]} \tag{28}$$

$$Ho_{2r+1}^{(1,2)}(s_n,\xi) = \frac{(-1)^r}{\sqrt{\frac{\sqrt{s_n}}{2} e^{\xi}}} e^{\pm i\left[\frac{\sqrt{s_n}}{2} e^{\xi} - \frac{3\pi}{4}\right]} \tag{29}$$

$$Ho_{2r+2}^{(1,2)}(s_n,\xi) = \frac{(-1)^{r+1}}{\sqrt{\frac{\sqrt{s_n}}{2} e^{\xi}}} e^{\pm i\left[\frac{\sqrt{s_n}}{2} e^{\xi} - \frac{\pi}{4}\right]} \tag{30}$$

Derivatives of the radial solutions may be found by differentiating equations (21) through (24) and using the Bessel Function identities for derivatives

$$H_p'(x) = H_{p-1}(x) - \frac{p}{x} H_p(x) \tag{31}$$

$$H_p'(x) = -H_{p+1}(x) + \frac{p}{x} H_p(x) \tag{32}$$

The general separable solution for $p_n(\xi,\eta)$ may now be given as

$$p_n(\xi,\eta) = \sum_{r=0}^{\infty}\left\{\left[A_{nr}^{(1)} He_r^{(1)}(s_n,\xi) + A_{nr}^{(2)} H_{er}^{(2)}(s_n,\xi)\right] Se_r(s_n,\eta) + \left[B_{nr}^{(1)} Ho_r^{(1)}(s_n,\xi) + B_{nr}^{(2)} Ho_r^{(2)}(s_n,\xi)\right] So_r(s_n,\eta)\right\} \tag{33}$$

$p_n(\xi,\eta)$ and $p_{(-n)}(\xi,\eta)$ must be conjugate functions in order for $p(\xi,\eta,t)$ to be real. This condition introduces the following constraints on the undetermined coefficients of equation (33)

$$\left.\begin{aligned} A^{(1)}_{-nr} &= \overline{(A^{(2)}_{nr})} && (34a)\\ A^{(2)}_{-nr} &= \overline{(A^{(1)}_{nr})} && (34b)\\ B^{(1)}_{-nr} &= \overline{(B^{(2)}_{nr})} && (34c)\\ B^{(2)}_{-nr} &= \overline{(B^{(1)}_{nr})} && (34d)\end{aligned}\right\} \quad n = 1,2,3 \ldots$$

Equations (34) show that it is sufficient to determine the complex coefficients for positive values of n only.

Substituting (33) into 4.2(1) and using the asymptotic formula for the radial Mathieu functions gives a far-field pressure formula

$$p(\xi,\eta,t) = \sum_{n=-\infty}^{\infty} \sum_{r=0}^{\infty} \frac{(-1)^r}{\sqrt{\frac{\sqrt{s_n}}{2}\, e^{\xi}}} \left\{ \left[A^{(1)}_{nr}\, e^{i\left[n(ke^{\xi}+t)-\theta_r\right]} + A^{(2)}_{nr}\, e^{-i\left[n(\eta e^{\xi}-t)-\theta_r\right]} \right] Se_r(\eta) + \left[B^{(1)}_{nr}\, e^{i\left[n(ke^{\xi}+t)-\theta_r\right]} + B^{(2)}_{nr}\, e^{-i\left[n(ke^{\xi}-t)-\theta_r\right]} \right] So_r(\eta) \right\} \tag{35}$$

where

$$\theta_r = \begin{cases} \frac{\pi}{4}, & r \text{ even} \\ \frac{3\pi}{4}, & r \text{ odd} \end{cases}$$

This equation clearly shows that the coefficients $A^{(2)}_{nr}$ and $B^{(2)}_{nr}$ must be associated with diverging waves, while $A^{(1)}_{nr}$ and $B^{(1)}_{nr}$ are associated with converging waves.

It is often convenient to work with the real and imaginary parts of the radial solutions. In reference 42, these are defined as

$$He_r^{(1)}(s_n,\xi) = Je_r(s_n,\xi) + iNe_r(s_n,\xi) \tag{36}$$

$$Ho_r^{(1)}(s_n,\xi) = Jo_r(s_n,\xi) + iNo_r(s_n,\xi) \tag{37}$$

The Wronskian of these solutions may be shown to be equal to 1. Therefore

$$Je_r Ne_r' - Ne_r Je_r' = 1 \tag{38}$$

and

$$Jo_r No_r' - No_r Jo_r' = 1 \tag{39}$$

for all values of s_n, r, and ξ. (40)

Finally, it may be seen from equations (21) to (24) that Je_r and Jo_r are even and odd functions, respectively. Ne_r and No_r, however, are neither even nor odd.

4.3 Interior Cylinder Problem

The pressure within the cylinder is given by substituting 4.2.2(33) into 4.2(1)

$$p^i(\xi,\eta,t) = \sum_{n=-\infty}^{\infty} \sum_{r=0}^{\infty} \Big\{ \left[A_{nr}^{(1)} He_r^{(1)} + A_{nr}^{(2)} He_r^{(2)}\right] Se_r + \left[B_{nr}^{(1)} Ho_r^{(1)} + B_{nr}^{(2)} Ho_r^{(2)}\right] So_r \Big\} e^{int} \tag{1}$$

In order for the pressure and its gradient to be continuous on the x-axis ($\xi = 0$),

$$p^i(0,\eta,t) = p^i(0,-\eta,t) \tag{2}$$

and

$$\frac{\partial p^i(0,\eta,t)}{\partial \xi} = \frac{-\partial p\ (0,-\eta,t)}{\partial \xi} \tag{3}$$

By using the orthogonality equations of the complex exponential and of the circumferential Mathieu functions, conditions (2) and (3) may be shown to be equivalent to

$$A_{nr}^{(1)} = A_{nr}^{(2)} \tag{4}$$

$$B_{nr}^{(1)} = B_{nr}^{(2)} \tag{5}$$

Let the velocity normal to the surface of the cylinder be given by the expansion

$$q_\xi(\xi_o,\eta,t) = \frac{\sum_{n=-\infty}^{\infty} \sum_{r=0}^{\infty} (U_{nr}Se_r(\eta) + V_{nr}So_r(\eta))e^{int}}{\sqrt{2k^2(\cosh 2\xi_o - \cos 2\eta)}} \tag{6}$$

If equations 4.2(3) and (1) are used to compute the velocity at the surface and the result is equated to the expression in (6), then two relations are obtained for the A_{nr} and B_{nr} coefficients.

$$2A_{nr}^{(1)} Je_r'(s_n, \xi_o) = -inU_{nr} \tag{7}$$

$$2B_{nr}^{(1)} Jo_r'(s_n, \xi_o) = -inV_{nr} \tag{8}$$

By using equations (4), (5), (7), and (8) to eliminate the coefficients A_{nr} and B_{nr} from equation (1), we obtain

$$p^i(\xi,\eta,t) = -\sum_{n=-\infty}^{\infty} in \sum_{r=0}^{\infty} \left\{ \alpha_{nr}^i(\xi) U_{nr} Se_r(\eta) + \beta_{nr}^i V_{nr} So_r(\eta) \right\} e^{int} \tag{9}$$

where

$$\alpha_{nr}^i = \frac{Je_r(\xi)}{Je_r'(\xi_o)} \tag{10}$$

and

$$\beta_{nr}^i = \frac{Jo_r(\xi)}{Jo_r'(\xi_o)} \tag{11}$$

4.4 Exterior Cylinder Problem

Consider a periodic wave which is moving in the positive sense along the line

$$x + iy = R\, e^{i\alpha} \tag{1}$$

This wave may be expressed as

$$p(\xi,\eta,t) = \sum_{n=-\infty}^{\infty} P_n\, e^{in(t-R)} \tag{2}$$

The normal distance from the origin to a point on the wave is given by

$$R = x \cos \alpha + y \sin \alpha \tag{3}$$

or

$$nR = \sqrt{s_n}(\cosh \xi \cos \eta \cos \alpha + \sinh \xi \sin \eta \sin \alpha) \tag{4}$$

It is desired to represent this plane wave in the form of equation (63), thus we write the tentative expansion

$$e^{-inr} = \sum_{r=0}^{\infty} \left\{ \left[E_{nr}^{(1)} He_r^{(1)} + E_{nr}^{(2)} He_r^{(2)} \right] Se_r + \left[F_{nr}^{(1)} Ho_r^{(1)} + Fo_r^{(2)} Ho_r^{(2)} \right] So_r \right\} \tag{5}$$

The orthogonality conditions on the periodic Mathieu functions yield simultaneous equations

$$N_r \left[E_{nr}^{(1)} He_r^{(1)} + E_{nr}^{(2)} He_r^{(2)} \right] = \int_0^{2\pi} e^{-inR} Se_r(\eta) d\eta \tag{6}$$

$$N_r' \left[F_{nr}^{(1)} Ho_r^{(1)} + F_{nr}^{(2)} Ho_r^{(2)} \right] = \int_0^{2\pi} e^{-inR} So_r(\eta) d\eta \tag{7}$$

The exponential term in equations (79) and (80) satisfies the wave equation, and since R is invariant when α and η are interchanged

$$\frac{\partial^2 e^{-inR}}{\partial \alpha^2} = \frac{\partial^2 e^{-inR}}{\partial \eta^2} \tag{8}$$

Therefore, the integral term in (6) satisfies both Mathieu equations

$$\frac{d^2y}{d\alpha^2} + (be_r - s_n \cos^2 \alpha) y = 0 \tag{9}$$

and

$$\frac{d^2y}{d\xi^2} - (be_r - s_n \cosh^2 \xi)\, y = 0 \tag{10}$$

Similarly the integral in equation (7) would satisfy equations (9) and (10) if be_r was replaced by bo_r. Now, since the integrals satisfy the separated equations, they must be proportional to products of the solutions of these equations. Also, the integrals are periodic in $i\xi$, so the product solutions must have this periodicity. Consequently,

$$\int_0^{2\pi} e^{-inR} Se_r(\eta)d\eta = \rho e_r Se_r(\alpha) Je_r(\xi) \tag{11}$$

$$\int_0^{2\pi} e^{-inR} So_r(\eta)d\eta = \rho o_r So_{r(\alpha)} Jo_r(\xi) \tag{12}$$

$Je_r(\xi)$ and $Jo_r(\xi)$ are given as series involving only Bessel functions of the first kind, which is why the combinations in (11) and (12) are periodic in $i\xi$.

To evaluate ρe_r set $\alpha = 0$ and develop the left sides of equation (11) in a Bessel function series by using the series definition of se_r, and the integral definition of the Bessel function (ref. 51).

$$J_n(Z) = \frac{1}{2\pi i^n} \int_0^{2\pi} e^{iZ \cos \theta} \cos n\theta \, d\theta \tag{13}$$

Then evaluate this equation for large values of ξ by using the asymptotic formulas for the Bessel functions, equations 4.2.2(27) through 4.2.2(30).

The result is

$$\rho e_r = (-i)^r \sqrt{8\pi} \tag{14}$$

To evaluate ρo_r, first differentiate equation (12) with respect to α. Then proceed as above to obtain the result

$$\rho o_r = (-i)^r \sqrt{8\pi} \tag{15}$$

We may now use equations (11) and (12) with equations (6) and (7) to solve for the expansion coefficients in equation (5). They are

$$E_{nr}^{(1)} = E_{nr}^{(2)} = \frac{(-i)^r \sqrt{8\pi}\, Se_r(\alpha)}{2N_r} \tag{16}$$

$$F_{nr}^{(1)} = F_{nr}^{(2)} = \frac{(-1)^r \sqrt{8\pi}\, \rho o_r So_r(\alpha)}{2N_r'} \tag{17}$$

Thus the elliptical wave representation of the plane wave is

$$e^{-inR} = \sqrt{8\pi} \sum_{r=0}^{\infty} (-i)^r \left[\frac{Se_r(\alpha)}{N_r} Je_r(\xi) Se_r(\eta) + \frac{So_r(\alpha)}{N_r'} Jo_r(\xi) So_r(\eta) \right] \tag{18}$$

The expansion for e^{inR} is simply the conjugate of equation (18).

The pressure in the exterior of the cylinder is

$$p^o(\xi,\eta,t) = \sum_{n=-\infty}^{\infty} \sum_{r=0}^{\infty} \left\{ \left[C_{nr}^{(1)} He_r^{(1)} + C_{nr}^{(2)} He_r^{(2)} \right] Se_r + \left[D_{nr}^{(1)} Ho_r^{(1)} + D_{nr}^{(2)} Ho_r^{(2)} \right] So_r \right\} e^{int} \tag{19}$$

Since the external pressure field is composed of outward-traveling scattered waves and the incident plane wave, it may be seen, by comparing (19) to 4.2.2(35), that

$$C_{nr}^{(1)} = D_{nr}^{(1)} = 0, \quad n = 1,2,3 \ldots \tag{20}$$

Therefore

$$p_n^o(\xi,\eta) = \sum_{r=0}^{\infty}\left\{\left[C_{nr}^{(2)}He_r^{(2)}(\xi) + (-i)^r\sqrt{8\pi}\,\rho_n\frac{Se_r(\alpha)}{N_r}\,Je_r(\xi)\right]Se_r(\eta)\right.$$

$$\left. + \left[D_{nr}^{(2)}Ho_r^{(2)}(\xi) + (-i)^r\sqrt{8\pi}\,\rho_n\,\frac{So_r(\alpha)}{N_r'}\,Jo_r(\xi)\right]So_r(\eta)\right\} \tag{21}$$

Since the normal velocity is continuous at the cylinder surface, equations 4.3(6) and (21) may be used to solve for $C_{nr}^{(2)}$ and $D_{nr}^{(2)}$.

$$C_{nr}^{(2)} = \frac{-1}{He_r^{(2)\prime}(\xi_o)}\left[inU_{nr} + (-i)^r\sqrt{8\pi}\,\rho_n\,\frac{Se_r(\alpha)}{N_r}\,Je_r'(\xi_o)\right] \tag{22}$$

$$D_{nr}^{(2)} = \frac{-1}{Ho_r^{(2)\prime}(\xi_o)}\left[inV_{nr} + (-i)^r\sqrt{8\pi}\,\rho_n\,\frac{So_r(\alpha)}{N_r'}\,Jo_r'(\xi_o)\right] \tag{23}$$

The external pressure field is found by substituting (21) through (23) into (19) to obtain

$$p^o(\xi,\eta,t) = -\sum_{n=-\infty}^{\infty}\sum_{r=0}^{\infty}\left\{in\left[\alpha_{nr}^o(\xi)U_{nr}Se_r(\eta) + \beta_{nr}^o\,V_{nr}So_r(\eta)\right]\right.$$

$$\left. + P_n\left[\Omega e_{nr}Se_r(\eta) + \Omega o_{nr}So_r(\eta)\right]\right\}e^{int} \tag{24}$$

where

$$\alpha_{nr}^o = \frac{He_r^{(2)}(\xi)}{He_r^{(2)\prime}(\xi_o)} \tag{25}$$

$$\beta_{nr}^o = \frac{Ho_r^{(2)}(\xi)}{Ho_r^{(2)\prime}(\xi_o)} \tag{26}$$

$$\Omega e_{nr} = \frac{i(-i)^r \sqrt{8\pi}\ Se_r(\alpha)}{N_r He_r^{(2)\prime}(\xi_o)} \tag{27}$$

$$\Omega o_{nr} = \frac{i(-i)^r \sqrt{8\pi}\ So_r(\alpha)}{N_r' Ho_r^{(2)\prime}(\xi_o)} \tag{28}$$

For negative values of n, the conjugates of equation (25) through (28) are used in the pressure equation.

4.5 Porous Cylinder Problem

The interior and exterior solutions have both been given in terms of velocity normal to the cylinder surface, that is, in terms of the coefficients U_{nr} and V_{nr}. Equation 4.1(11), which relates pressure drop and velocity at the cylinder, will now be used to obtain equations which determine these coefficients.

The pressure drop may be found from the interior solution, equation 4.3(9), and the exterior solution, equation 4.4(24). When these are used with 4.1(11), it becomes

$$\sum_{n=-\infty}^{\infty} \sum_{r=0}^{\infty} \left\{ \left[in\alpha_{nr}U_{nr} + Fe_{nr} \right] Se_r(\eta) + \left[in\beta_{nr}V_{nr} + Fo_{nr} \right] So_r(\eta) \right\} e^{int}$$

$$= \rho_A \frac{\partial q_\xi(\xi_o, \eta, t)}{\partial t} + \frac{\Delta P}{\epsilon} \left\{ \epsilon q_\xi \right\} \tag{1}$$

where

$$\alpha_{nr} = \alpha_{nr}^o(\xi_o) - \alpha_{nr}^i(\xi_o) = \frac{i}{Je_r(s_n, \xi_o) He_r^{(2)\prime}(s_n, \xi_o)} \tag{2}$$

$$\beta_{nr} = \beta_{nr}^o(\xi_o) - \beta_{nr}^i(\xi_o) = \frac{i}{Jo_r'(s_n, \xi_o) Ho_r^{(2)\prime}(s_n, \xi_o)} \tag{3}$$

$$Fe_{nr} = P_n \Omega e_{nr}(\xi_o) \tag{4}$$

and

$$Fo_{nr} = P_n \Omega o_{nr}(\xi_o) \tag{5}$$

Since q_ξ is given in terms of U_{nr} and V_{nr} by 4.3(6), equation (1) may be used to solve for these coefficients. The solution of this equation is the fundamental problem for finding the scattering from a porous cylinder. By applying the orthogonality relations for the complex exponentials and Mathieu functions, equation (1) may be reduced to infinite sets of nonlinear algegraic equations.

$$N_l(im\alpha_{ml}U_{ml} + Fe_{ml}) = im\rho_A \sum_{r=0}^{\infty} M_{lr}U_{mr}$$

$$+ \frac{1}{2\pi}\int_0^{2\pi}\int_0^{2\pi} e^{-imt} Se_l(\eta)\frac{\Delta P}{\epsilon}\left\{\epsilon q_\xi(\eta,t)\right\} d\eta\, dt \tag{6}$$

and

$$N_l'(im\beta_{ml}V_{ml} + Fo_{ml}) = im\rho_A \sum_{r=0}^{\infty} N_{lr}V_{mr}$$

$$+ \frac{1}{2\pi}\int_0^{2\pi}\int_0^{2\pi} e^{-imt} So_l(\eta)\frac{\Delta P}{\epsilon}\left\{\epsilon q_\xi\right\} d\eta\, dt \tag{7}$$

where

$$M_{lr} = \int_0^{2\pi} \frac{Se_l(\eta)Se_r(\eta)d\eta}{\sqrt{2k^2(\cosh 2\xi_o - \cos 2\eta)}} \tag{8}$$

$$N_{lr} = \int_0^{2\pi} \frac{Se_l(\eta)Se_r(\eta)d\eta}{\sqrt{2k^2(\cosh 2\xi_o - \cos 2\eta)}} \tag{9}$$

In equations (6) and (7), it must be noted that all Mathieu functions and parameters in the mth equation depend on the parameter s_m (eq. 4.2(8)).

4.5.1 Power Series Equations for Porous Cylinder

As in the one-dimensional problem, let

$$\frac{\Delta P}{\epsilon}\left\{\epsilon q_\xi\right\} = Rq_\xi + \delta\Gamma\left\{q_\xi\right\} \tag{1}$$

and

$$q_\xi \sim q_\xi^{(0)} + \delta q_\xi^{(1)} + \ldots \tag{2a}$$

$$U_{nr} \sim U_{nr}^{(0)} + \delta U_{nr}^{(1)} + \ldots \tag{2b}$$

$$V_{nr} \sim V_{nr}^{(0)} + \delta V_{nr}^{(1)} + \ldots \tag{2c}$$

then $q_\xi^{(0)}$ is given by

$$q_\xi^{(0)}(\eta,t) = \sum_{n=-\infty}^{\infty}\sum_{r=0}^{\infty} \frac{(U_{nr}^{(0)}Se_r(\eta) + V_{nr}^{(0)}So_r(\eta))e^{int}}{\sqrt{2k^2(\cosh 2\xi_o - \cos 2\eta)}} \tag{3}$$

With these changes, equations 4.5(6) and 4.5(7) are converted into

$$\left.\begin{aligned} N_l\left(im\alpha_{ml}U_{ml}^{(j)} + Fe_{ml}^{(j)}\right) &= (R + im\rho_A)\sum_{r=0}^{\infty} M_{lr}(s_m)U_{mr}^{(j)} \qquad (4)\\ N_l'\left(im\beta_{ml}V_{ml}^{(j)} + Fo_{ml}^{(j)}\right) &= (R + im\rho_A)\sum_{r=0}^{\infty} N_{lr}(s_m)V_{mr}^{(j)} \qquad (5)\end{aligned}\right\} j = 0,1$$

In equations (4) and (5) the forcing terms are

$$Fe_{ml}^{(0)} = Fe_{ml} \tag{6a}$$

$$Fo_{ml}^{(0)} = Fo_{ml} \tag{6b}$$

$$Fe_{ml}^{(1)} = -\frac{1}{2\pi N_l}\int_0^{2\pi}\int_0^{2\pi} e^{-imt} Se_l(s_m,\eta) r\left\{q_\xi^{(0)}(\eta,t)\right\} dt\, d\eta \tag{7a}$$

and

$$Fo_{ml}^{(1)} = -\frac{1}{2\pi N_l'}\int_0^{2\pi}\int_0^{2\pi} e^{-imt} So_l(s_m,\eta) r\left\{q_\xi^{(0)}(\eta,t)\right\} dt\, d\eta \tag{7b}$$

The power series approximation thus reduces the problem to the solution of infinite sets of linear algebraic equations. The solution to these equations are easily approximated by truncating them to obtain finite sets of equations. Solving the zeroth-order equations involves a matrix inversion and use of the forcing function which depends on the incident plane wave. The first-order solution uses the same inverse matrix and a forcing function which depends on the zeroth-order solution (eq. (7a) and (7b)).

In Appendix A, the integrals M_{lr} and N_{lr} are evaluated, and it is shown that these integrals are zero unless both Mathieu functions in the integral have the same period. Equations (4) and (5) thus divide naturally into four sets of equations; one set for each type of circumferential Mathieu function.

$$N_{2l}\left(im\alpha_{m,2l}U_{m,2l}^{(j)} + Fe_{m,2l}^{(j)}\right) = Z_m \sum_{r=0}^{\infty} M_{2l,2r}U_{m,2r}^{(j)} \tag{8}$$

$$N_{2l+1}\left(im\alpha_{m,2l+1}U^{(j)}_{m,2l+1} + Fe^{(j)}_{m,2l+1}\right) = Z_m \sum_{r=0}^{\infty} M_{2l+1,2r+1}U^{(j)}_{m,2r+1} \tag{9}$$

$$N'_{2l+1}\left(im\beta_{m,2l+1}V^{(j)}_{m,2l+1} + Fo^{(j)}_{m,2l+1}\right) = Z_m \sum_{r=0}^{\infty} N_{2l+1,2r+1}V^{(j)}_{m,2r+1} \tag{10}$$

$$N'_{2l+2}\left(im\beta_{m,2l+2}V^{j}_{m,2l+2} + Fo^{(j)}_{m,2l+2}\right) = Z_m \sum_{r=0}^{\infty} N_{2l+2,2r+2}V^{(j)}_{m,2r+2} \tag{11}$$

where

$$Z_m = R + im\rho_A \tag{12}$$

Equations (8) through (11) are four infinite sets of linear equations. Their solutions may be approximated by truncating the sets to obtain a finite number of equations (ref. 54).

4.6 Variable Linear Impedance

There is a remarkable case of variable material properties where equation 4.5(1) may be reduced to uncoupled sets of equations. Note that if

$$\rho_A = \rho'_A \sqrt{2k^2(\cosh 2\xi - \cos 2\eta)} \tag{1}$$

and

$$\frac{\Delta P}{\epsilon}(\epsilon q_\xi) = R' \sqrt{2k^2(\cosh 2\xi - \cos 2\eta)}\, q_\xi, \tag{2}$$

then the procedures described in 4.5 would result in the solution

$$U_{nr} = \frac{Fo_{nr}}{Z'_n - in\beta_{nr}} \tag{3}$$

$$V_{nr} = \frac{Fo_{nr}}{Z'_n - in\beta_{nr}} \tag{4}$$

where

$$Z_n' = R' + in\rho_A' \tag{5}$$

4.7 Dissipation and Scattering Formulas

Once the velocity at the cylinder surface is obtained, the pressure or velocity at any point may be computed. Some other quantities of interest are the incident power, the scattered and dissipated power, and the far-field rms pressure. The derivation of these formulas is tedious, but routine, and only final results are given here.

The projected width which the oncoming plane wave "sees" is

$$w = h\sqrt{2(\cosh 2\xi - \cos 2\alpha)}\ , \tag{1}$$

and the power which would pass through this width due to the plane wave alone is

$$P_I = 2w \sum_{n=1}^{\infty} \left|P_n\right|^2 \tag{2}$$

The power of the outgoing waves alone is

$$P_s = 2 \sum_{n=1}^{\infty} \frac{1}{n} \sum_{r=0}^{\infty} \left\{ \left|C_{nr}^{(2)}\right|^2 N_r(s_n) + \left|D_{nr}^{(2)}\right|^2 N_r'(s_n) \right\} . \tag{3}$$

The rate of energy dissipation within the porous material is

$$P_d = \sum_{n=-\infty}^{\infty} \sum_{r=0}^{\infty} \left\{ \left[in\alpha_{nr} \left|U_{nr}\right|^2 N_r(s_n) + in\beta_{nr} \left|V_{nr}\right|^2 N_r'(s_n) \right.\right.$$

$$\left.\left. + \ Fe_{nr}U_{-nr}N_r(s_n) + Fo_{nr}V_{-nr}N_r'(s_n) \right] \right\} \tag{4}$$

at large distances from the cylinder where $\xi = \psi \gg 1$, the rms pressure is given by

$$\frac{e^{\frac{\psi}{2}}}{2} p_{rms}(\psi,\eta) \sim \left\{ \sum_{n=1}^{\infty} \frac{1}{\sqrt{s_n}} \left| \sum_{r=1}^{\infty} (-1)^r \left[C^{(2)}_{n(2r-2)} Se_{2r-2}(s_n,\eta) + iC^{(2)}_{n(2r-1)} Se_{2r-1}(s_n,\eta) \right.\right.\right.$$

$$\left.\left.\left. + iD^{(2)}_{n(2r-1)} So_{2r-1}(s_n,\eta) - D^{(2)}_{n(2r)} So_{2r}(s_n,\eta) \right] \right|^2 \right\}^{1/2} \qquad (5)$$

V. RESULTS AND DISCUSSION

5.1 Linearized Perturbation Theory

Measured data for the pressure-drop function for a typical sample of material are shown on figure 6. For comparison, straight lines representing acoustic resistances of 0.20, 0.66, and 1.0 are also shown. Each linear resistance curve may be thought of as an approximation to the material characteristic for a given sound intensity. This intensity is related to the value of ϵ. By referring to table I, it can be seen that the data of figure 6 are applicable for intensities in the 130 - 160 dB range. On figure 2, these data are plotted on a linear scale for three values of ϵ. Since the parameter δ characterizes the deviation of the pressure drop function from the linear curve, it may be seen from this figure that δ may be taken as $\sqrt{\epsilon}$.

In other words, for $\epsilon < 10^{-2}$, δ may be thought of as being large in comparison to ϵ, but small compared to 1. This amounts to saying the material nonlinearity becomes important before nonlinearity in the wave equation. However, there is no point in adding a δ^2 term to the power series equations for the material without also considering nonlinearities in the wave equation. Since the equations as derived in section 2.1 depended on ϵ being greater than 10^{-4}, there is a definite intensity range where the equations presented herein are valid. In terms of the decibel scale given in table I, this range is from about 120 dB to 160 dB. The complete theory could be described as having "zeroth order wave equations with first order linear boundary conditions in the kilohertzian region." This theory is the one used to develop the

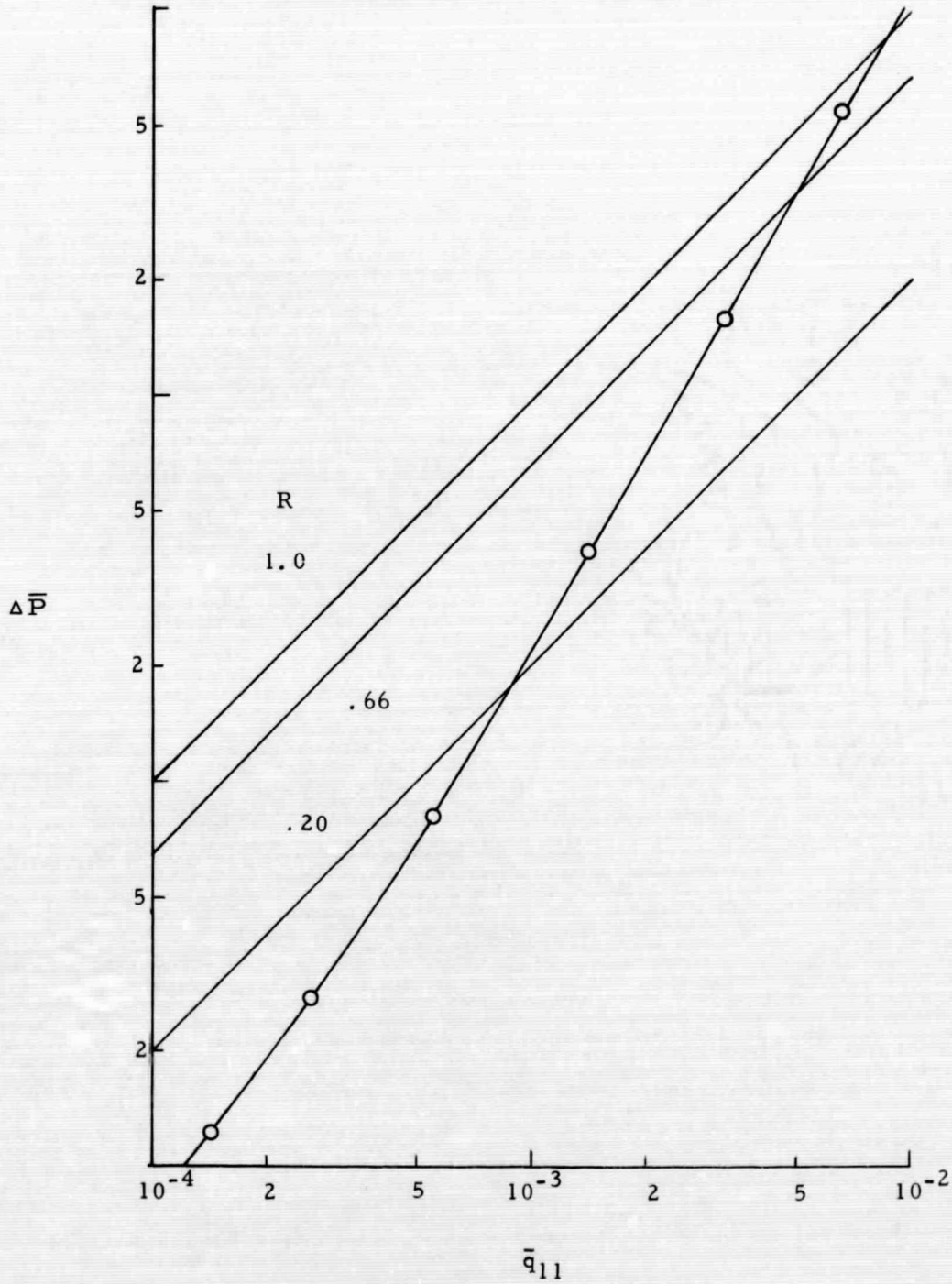

Figure 6.- Pressure drop function for typical fiber glass plastic porous material.

one-dimensional equations in section 3.3.3 and the two-dimensional equations in section 4.5.1.

5.2 Nonlinear Perturbation Theory

If the nonlinear pressure-drop function in 2.2(20) is not expanded in terms of the parameter δ, the theory then has zeroth order wave equations with nonlinear boundary conditions. Since the boundary conditions 2.2(19), 2.2(20) are accurate to ϵ^2, the solutions with this theory should be comparable to solutions with the linear perturbation theory described in section 5.1.

The one-dimensional problem depicted in figure 4(b) was used to compare the theories and methods of solutions. After obtaining the exact solution, the problem was solved numerically by the steepest descent procedure of section 3.3.1. A third solution was obtained by the linear perturbation equations of section 3.3.3.

The first harmonic of the velocity at the sample as given by the three methods of solution is shown on figure 7. The values of ϵ given correspond to incident wave intensities of 137, 151, and 157 dB. The decrease in velocity amplitude with intensity is due to the general steepening of the curves on figure 6. This is called increased acoustic resistance. Of course the actual velocity increases with ϵ, since the first term in 2.1(12d) has ϵ as a multiplier.

The "exact" and perturbation solutions correspond very well for the lowest value of ϵ and separate somewhat for larger values. Since the error in both solutions is of order ϵ^2, this separation is to be expected and confirms the earlier statement that the perturbation solution should

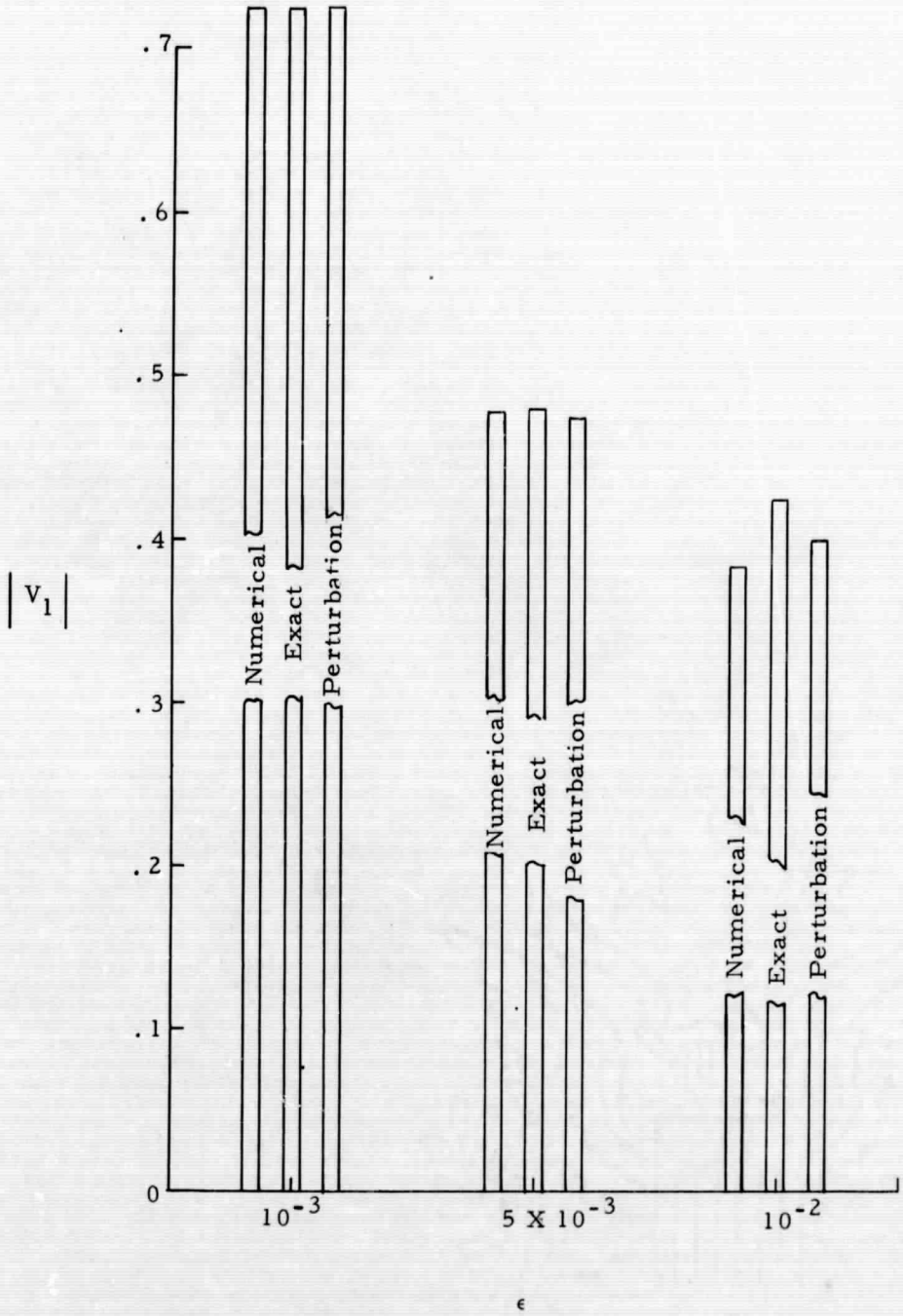

Figure 7.- Velocity amplitude predicted by exact and approximate solutions.

be limited to $\epsilon < 10^{-2}$. The correspondence between the steepest descent numerical procedure and the other solutions verifies this method, however, it seems to be no more accurate than the simpler perturbation procedure.

For problems other than the special one considered above, the "exact" solution is not available and a choice must be made between the numerical and perturbation method of solution. Since it is far easier to use, the perturbation technique seems the logical choice where it is valid.

5.3 Evaluation of Mathieu Functions

5.3.1 Coefficients and Periodic Mathieu Functions

Although the coefficients for the periodic Mathieu functions are tabulated over the range of s used in this paper (ref. 42), it was easier to program the computer to use the characteristic values to compute these coefficients than to read and interpolate the tables of coefficients. The method given by Blanch in reference 55 was used for this computation. Results were checked against the tables of coefficients and were found to check to eight significant figures. With this method of computation it is also possible to obtain the coefficients for $s > 100$ (which are not tabulated) from the tables of characteristic values for large s ($s > 100$) which are given in reference 42. With the coefficients available, the Fourier series in section 4.2.1 could be used for computation of the periodic solutions.

5.3.2 Radial Mathieu Functions

The evaluation of the radial Mathieu functions depends on computing the Bessel functions, J_n and Y_n. The Bessel functions of the first

kind were computed by Abramowitz's method, reference 56. In this method a unit value is assigned to J_k, where k is large compared to the argument of the Bessel function, J_{k+1} is taken as zero and then backward recurrence is used to find J_n for $n < k$. The normalization condition is then used to adjust the magnitude of the J_n's . Y_o is obtained from its series representation in terms of J_n, Y_1 is found from the Wronskian, and the rest of the Y_n's are found by forward recurrence. Bessel functions computed by this method were accurate to nine or ten significant figures for the range of arguments used.

Since there is little tabulated data available on the radial Mathieu functions, these were calculated by two different methods. The Bessel function product series given in section 4.2.2 were used and the series given by equations 3.03, 3.04, 3.15, and 3.16 in reference 42 were used for comparison. The latter series involve Bessel functions with argument $(\sqrt{s} \cosh \xi)$. Each series was checked at the origin (ξ=0) against the joining factors which are tabulated in reference 42. Also, each series was checked against the table of Barakat, Houston, and Levin, reference 30, and against the tables by Blanch and Clemm, reference 57, for $s = 4$. This was the upper limit (on s) of the available tables and the lower limit on s for this study.

The radial functions of the first kind were the most difficult to evaluate. The product series for $Je_0(4,0)$ checked against the NBS tables to seven significant figures. However, this accuracy decreased to one significant figure for $Je_6(4,0)$, and functions of higher order could not be computed by this method. The accuracy of the product series for the $Je(s,\xi)$ and $Jo(s,\xi)$ functions increased with s. $Je_0(100,0)$ was

accurate to nine figures, and $Je_{14}(100,0)$ retained a two figure accuracy.

The Bessel function series proved to be a superior method for computing Je and Jo. $Je_0(4,0)$ was given to seven figures by this method. Although this was not an improvement over the product series it was found that $Je_6(4,0)$ was accurate to six significant figures, which was an improvement of five significant figures over the product series. $Je_8(4,0)$ was accurate to five significant figures, but $Je_{10}(4,0)$ had only one significant figure and $Je_{12}(4,0)$, $Je_{14}(4,0)$ could not be computed. The accuracy of the Bessel series for $Je_r(s,0)$ also improved with increasing s. $Je_0(100,0)$ was accurate to six figures, and $Je_{14}(100,0)$ was accurate to eight figures. Note that the higher order functions are more accurate than the lower order functions when s is large. This turns out to be a very important property, since, in the scattering problem, the low-frequency (s=4) solutions require only the lower-order terms for convergence. The higher frequency solutions (s=100) require more terms, but it is no problem to compute these for the large values of s.

The radial functions of the second kind were computed by the product series. $Ne_r(4,0)$ and $No_r(4,0)$ were accurate to eight significant figures for $0 \leq r \leq 15$. The accuracy of the product series for $Ne_r(s,0)$ and $No_r(s,0)$ decreased with s. For example, $Ne_0(100,0)$ was only accurate to three significant figures. $Ne_{14}(100,0)$ had six figures accuracy; a loss of only two places.

The accuracy of both methods of computation improved with distance from the origin. This was established by comparing the results of each series and assuming that, if they were the same they were correct.

Larger values of ξ correspond to smaller values of cylinder eccentricity thus it is generally easier to evaluate the radial functions on a nearly circular cylinder than on a nearly flat cylinder.

In the problem of scattering from a porous cylinder, the product series were used to evaluate the functions of the second kind and their derivatives. The Bessel series were used to find the functions of the first kind, and the derivatives of these functions were found from the Wronskian relations 4.2.2(38,39).

The magnitude and phase of the complex radial Mathieu functions, He_r and Ho_r, could be computed to eight significant figures for $s=4$, and six figures for $s=100$. This is somewhat surprising in view of the above discussion of the accuracy of the functions of the first and second kinds which are, respectively, the real and imaginary parts of the complex function. Luckily, it turns out that the inaccurate part of the complex number is much less in magnitude than the accurate part, so that the complex representation of the number is fairly good throughout the range of s.

5.3.3 Evaluation of Coefficients and Integrals

The evaluation of the coefficients in the scattering equations of section 4.5 depends directly on the evaluation of the Mathieu functions. The coefficients given by 4.5(2,3) are only as accurate as the derivative of the radial function of the first kind. As noted in the previous section, this could be computed to five significant figures for $s=4$ and orders up to eight. At $s=100$, the function of the first kind could be determined to six figures for all orders, but the function of the second

kind could only be obtained to three figures for the lower orders. Since the Wronskian was used to solve for the derivative, the derivative is limited to three figure accuracy. Improved accuracy for this derivative may have been obtained (at s=100) by differentiating the Bessel series for the function. Note that the accuracy problem is associated with the waves within the cylinder. The coefficients for the exterior field, 4.4(25,26), may always be found to six significant figures.

The nonhomogeneous terms, 4.5(4,5) may be computed to six significant figures since they involve only the complex radial functions and the periodic functions. The normalizing factors; N_r and N_r' are computed from the coefficients De_r, Do_r and so are accurate to eight figures.

Computation of the coupling coefficients, $M_{\ell r}$ and $N_{\ell r}$ is discussed in appendix A. The series presented there were used to evaluate these. The integrals, I_{2m}, were computed to eight significant figures to obtain eight-figure accuracy for the coupling terms.

The nonhomogeneous terms in the first-order perturbation solution were computed by numerically taking the double Fourier transform of $\Gamma\left\{q_\xi(\eta,t)\right\}$ in equations 4.5.1(7a,7b) and expressing the periodic functions in these equations by their Fourier series so that term-by-term integration could be used to find $Fe_{m\ell}^{(1)}$ and $Fo_{m\ell}^{(1)}$. The accuracy of this was checked by solving a linear problem by two methods. The problem where $\frac{\Delta P}{\epsilon}\left\{\epsilon q_\xi\right\} = q_\xi$, $\Gamma\left\{q_\xi\right\} = 0$, was first solved. In the second method, $\frac{\Delta P}{\epsilon}\left\{\epsilon q_\xi\right\} = 0.9q_\xi$, and $\Gamma\left\{q_\xi\right\} = 0.1q_\xi$ was used. Since the two problems are physically identical, the solutions must correspond if the numerical work is correctly programmed. It was found that the solutions did match to two significant figures, which is what should be expected for $\delta=0.1$.

5.4 Scattering from a Porous Cylinder

5.4.1 Linear Boundary Conditions

In order to get some general information about the effects of different parameters, solutions were first obtained with linear boundary conditions. Focal distances, h, of 2, 4, 6, 8, and 10 were used to determine the effect of frequency. These values correspond to cylinder lengths of about 1/2 wavelength to over 3 wavelengths. Solutions were made for acoustic resistances of 1, 2, and 4. The angle of incidence was varied in 30° increments from 0° to 90°, and the radial coordinate, ξ, was taken as 0.2, 0.4, and 0.80. Tables II through VI give the ratios of scattered and dissipated power to incident power for these cases.

The ratio of scattered power to incident power, SR, varied from about 0.04 to over 1.0. It was a minimum for grazing incidence and maximum for normal incidence and increased monotonically with resistance. As the resistance becomes infinite, the SR must approach the value for the hard cylinder. A computation was made for the case of the hard cylinder to check against the work of Barakat, reference 28. It was noted that the values agreed for normal incidence but differed by a factor of 2 for grazing incidence. Although it has not been possible to find the reason for this discrepency, a possible explanation could be the errors which are apparent in table I of Barakat's paper.

The ratio of the dissipated energy to the incident energy, DR, must have a maximum value between $R=0$, and $R=\infty$. The DR depends on the product of the pressure drop and velocity at the cylinder surface. For zero resistance, the pressure drop is zero, and for the infinite

TABLE II.- SCATTERED AND DISSIPATED POWER RATIOS, $h = 2.0$

R		1		2		4	
ξ	α	SR	DR	SR	DR	SR	DR
0.2	0	0.039	0.545	0.094	0.751	0.158	0.771
	30	0.146	0.599	0.304	0.635	0.474	0.542
	60	0.294	0.713	0.601	0.762	0.946	0.629
	90	0.376	0.721	0.744	0.770	1.179	0.654
0.4	0	0.115	0.663	0.233	0.820	0.349	0.788
	30	0.176	0.694	0.371	0.792	0.583	0.695
	60	0.275	0.799	0.583	0.860	0.936	0.704
	90	0.316	0.828	0.661	0.869	1.609	0.697
0.8	0	0.202	0.750	0.415	0.922	0.659	0.851
	30	0.236	0.730	0.479	0.866	0.764	0.771
	60	0.321	0.635	0.612	0.695	0.938	0.586
	90	0.375	0.553	0.681	0.570	1.008	0.470

TABLE III.- SCATTERED AND DISSIPATED POWER RATIOS, $h = 4.0$

R		1		2		4	
ξ	α	SR	DR	SR	DR	SR	DR
0.2	0	0.050	0.585	0.122	0.860	0.218	1.03
	30	0.161	0.647	0.375	0.797	0.617	0.763
	60	0.312	0.762	0.654	0.827	1.069	0.697
	90	0.365	0.803	0.740	0.824	1.154	0.653
0.4	0	0.138	0.693	0.298	0.927	0.483	0.956
	30	0.202	0.703	0.437	0.872	0.742	0.828
	60	0.342	0.655	0.666	0.707	1.038	0.606
	90	0.414	0.597	0.765	0.604	1.139	0.498
0.8	0	0.255	0.639	0.505	0.803	0.808	0.801
	30	0.289	0.619	0.565	0.728	0.892	0.694
	60	0.324	0.674	0.642	0.744	1.005	0.652
	90	0.392	0.543	0.718	0.569	1.069	0.499

TABLE IV.- SCATTERED AND DISSIPATED POWER RATIOS, h = 6.0

R		1		2		4	
ξ	α	SR	DR	SR	DR	SR	DR
0.2	0	0.065	0.581	0.161	0.846	0.288	0.984
	30	0.165	0.670	0.395	0.852	0.732	0.835
	60	0.320	0.758	0.666	0.815	1.072	0.674
	90	0.390	0.747	0.760	0.773	1.165	0.621
0.4	0	0.181	0.590	0.377	0.728	0.599	0.697
	30	0.236	0.628	0.496	0.754	0.828	0.717
	60	0.358	0.637	0.695	0.685	1.076	0.592
	90	0.376	0.722	0.740	0.742	1.137	0.596
0.8	0	0.272	0.607	0.540	0.738	0.865	0.743
	30	0.291	0.632	0.584	0.734	0.932	0.700
	60	0.340	0.637	0.661	0.713	1.031	0.649
	90	0.377	0.599	0.706	0.661	1.074	0.605

TABLE V.- SCATTERED AND DISSIPATED POWER RATIOS, h = 8.0

R		1		2		4	
ξ	α	SR	DR	SR	DR	SR	DR
0.2	0	0.0692	0.454	0.171	0.636	0.308	0.710
	30	0.174	0.663	0.415	0.842	0.773	0.829
	60	0.359	0.667	0.708	0.716	1.109	0.611
	90	0.440	0.609	0.814	0.596	1.207	0.469
0.4	0	0.122	0.509	0.267	0.704	0.467	0.773
	30	0.261	0.596	0.531	0.713	0.869	0.704
	60	0.343	0.689	0.682	0.748	1.072	0.638
	90	0.424	0.591	0.785	0.585	1.165	0.466
0.8	0	0.188	0.546	0.411	0.700	0.726	0.738
	30	0.301	0.596	0.594	0.692	0.945	0.671
	60	0.337	0.637	0.660	0.713	1.033	0.648
	90	0.340	0.658	0.668	0.724	1.042	0.637

TABLE VI.- SCATTERED AND DISSIPATED POWER RATIOS- h = 10.0

R		1		2		4	
ξ	α	SR	DR	SR	DR	SR	DR
0.2	0	0.085	0.554	0.200	0.807	0.354	0.978
	30	0.186	0.631	0.432	0.795	0.790	0.795
	60	0.384	0.595	0.737	0.615	1.131	0.520
	90	0.429	0.648	0.800	0.664	1.200	0.548
0.4	0	0.193	0.582	0.414	0.735	0.688	0.756
	30	0.256	0.587	0.533	0.694	0.885	0.656
	60	0.374	0.601	0.721	0.630	1.106	0.530
	90	0.381	0.717	0.748	0.739	1.150	0.596
0.8	0	0.289	0.563	0.578	0.650	0.920	0.634
	30	0.304	0.601	0.608	0.686	0.971	0.648
	60	0.345	0.635	0.680	0.689	1.064	0.608
	90	0.338	0.716	0.687	0.766	1.087	0.647

resistance the velocity is zero, while the pressure differential must remain finite. It may be seen from the tables that the optimum resistance is usually around 2, except for grazing incidence on a thin cylinder where it is near 4. This large value of optimum resistance is a surprising result, since in one dimensional problems, a resistive impedance of 1 gives the maximum absorption. For thin cylinders, the DR was an increasing function of the angle of incidence for R=1, and a decreasing function of the angle for R=4. Another interesting result is that the maximum value for the DR is just slightly larger than one for grazing incidence on a thin cylinder. Thus, it may be concluded that the maximum percentage of energy which can be removed from sound propagating in a duct is equal to the percentage of duct area blocked by the splitter rings and spokes.

In the case of normal incidence, the dissipation by an elliptic cylinder should be roughly comparable to the dissipation by infinite parallel planes of porous material. If the length of the minor axis is held constant while the major axis is made large, then two sides of the cylinder will become nearly straight and parallel. This comparison is illustrated by figure 8. The data on this figure are for ξ=0.2 which corresponds to a cylinder whose major axis is roughly five times the minor axis. Dissipation ratios for the use of normal incidence are plotted against h, which may be interpreted as a frequency-parameter. The curves on figure 8 give the ratio of dissipated to incident energy for parallel planes whode spacing is equal to the cylinder's minor axis length. The maximum and minimum dissipations occur at very nearly the same frequencies for both the cylinder and parallel planes, and the

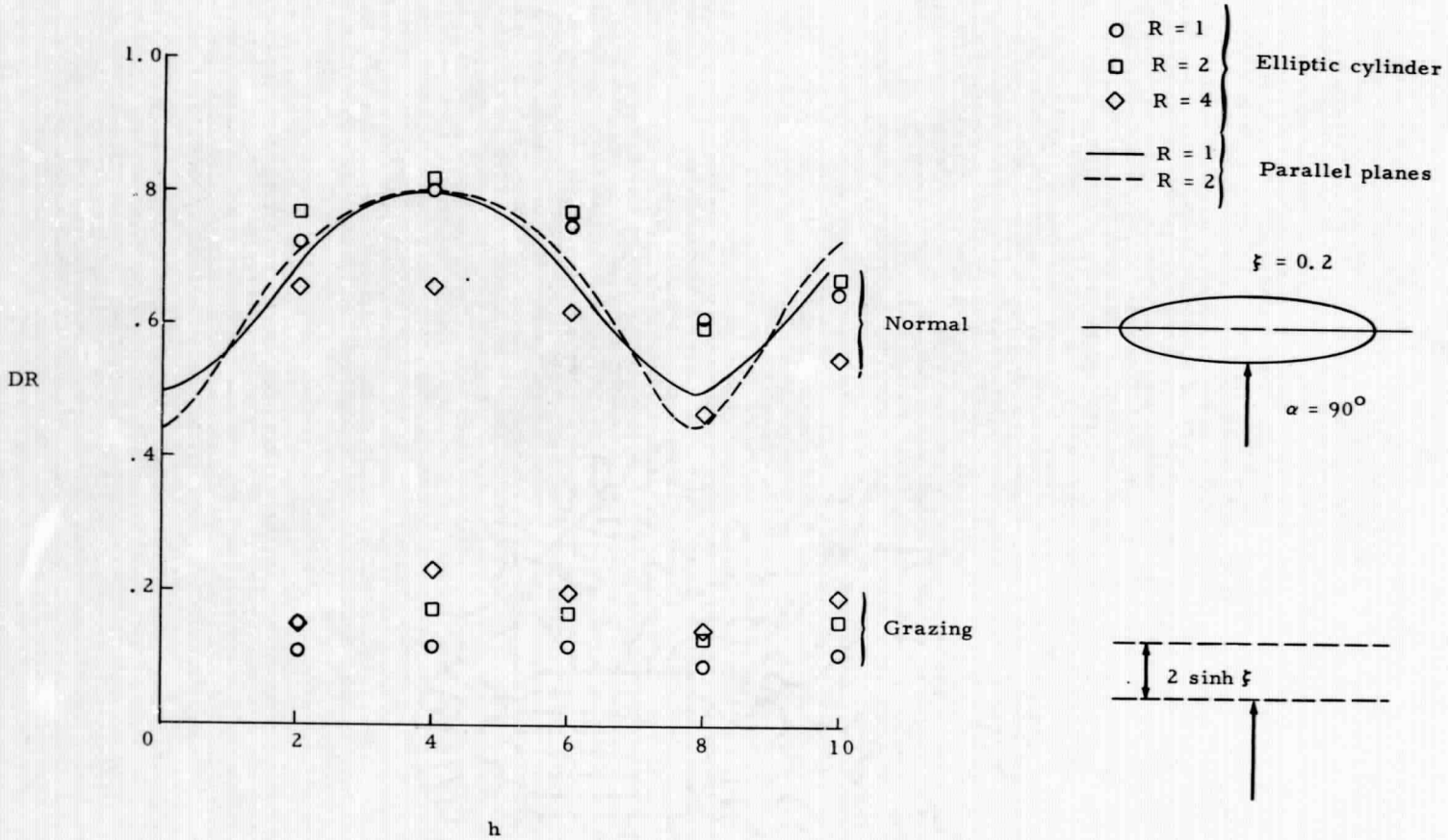

Figure 8.- Comparison of dissipation by elliptic cylinder and parallel planes.

maxima have nearly the same values. Data for grazing incidence are also shown on figure 8, however, instead of the DR, the ratio of energy dissipated to the energy in the normally incident wave is shown. This emphasizes the fact that only about one-fifth as much energy is dissipated from the grazing wave as from the normally incident wave. Again the maxima and minima occur at frequencies which correspond to the normal incidence case, which indicates that the minor axis length is the critical dimension for grazing wave energy dissipation. The maximum dissipation occurs when the minor axis is about 1/4 wavelength.

5.4.2 Nonlinear Boundary Conditions

It has been shown in reference 5 that high intensity waves tend toward a sawtooth form at large distances from the source. Because of this, the sawtooth has been used to illustrate high-intensity waves scattered by an elliptic cylinder. A five-term series approximation to the sawtooth wave was used, which gave five time harmonics of the fundamental frequency. Figure 9 shows the far-field rms pressure patterns for the linear solution and the first order power series solution for a grazing wave.

The value of ϵ was 10^{-2}, which corresponds to a sound intensity of about 160 dB. With this intensity, it can be seen from figure 2 that an acoustic resistance of 1 should be used for the linear solution. Figure 9 shows that the principle effect of the nonlinearity has been to increase the scattered pressure. This change in scattering should be on the order of 10 percent, since δ is 0.1. The curves on figure 9 are consistent with these conditions. The largest difference occurs near

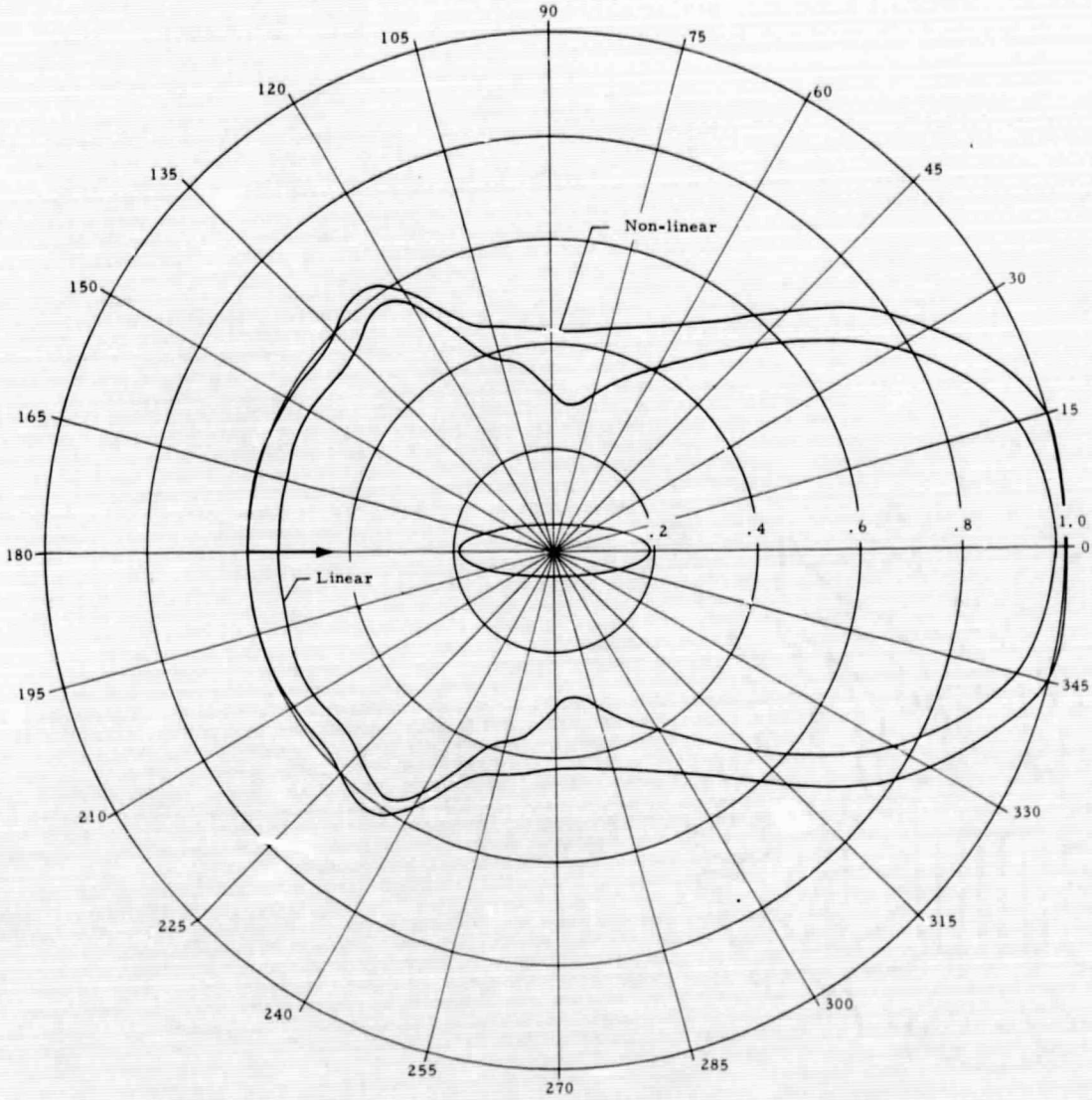

Figure 9.- Grazing incidence scattering of a sawtooth wave.

the sideline, with an increase of about 50 percent at $\eta=85^{\circ}$. Figure 10 shows the amplitude of the velocity as a function of position on the cylinder surface for the grazing incidence case. The peak velocities occur at the ends of the cylinder, where their value is about 0.95. This shows that the choice of ϵ and the resistance was realistic since the velocity varies between 0 and 1.

Also shown on figure 10 is the maximum deviation of the actual pressure drop from the pressure drop predicted by the linear resistance. Since it is always less than 0.2, it may be regarded as a perturbation. Again, this justify's the use of the power series technique for this problem.

Far-field pressure patterns for the normal incidence case are shown on figure 11. Although the only difference between this case and the previous one is angle of incidence, the large deviation between the patterns suggests a violation of the assumptions necessary for power series analysis. An inspection of the velocity amplitude at the surface for this case reveals that it has been underestimated by an order of magnitude. Consequently this solution is not valid. A better estimate of the true nonlinear solution would require a value of ϵ of 10^{-1}, but this is beyond the applicable range of this method, as was pointed out earlier. Thus, a solution for a 160 dB wave may be found for grazing incidence, but solutions must be restricted to lower intensities for normal incidence.

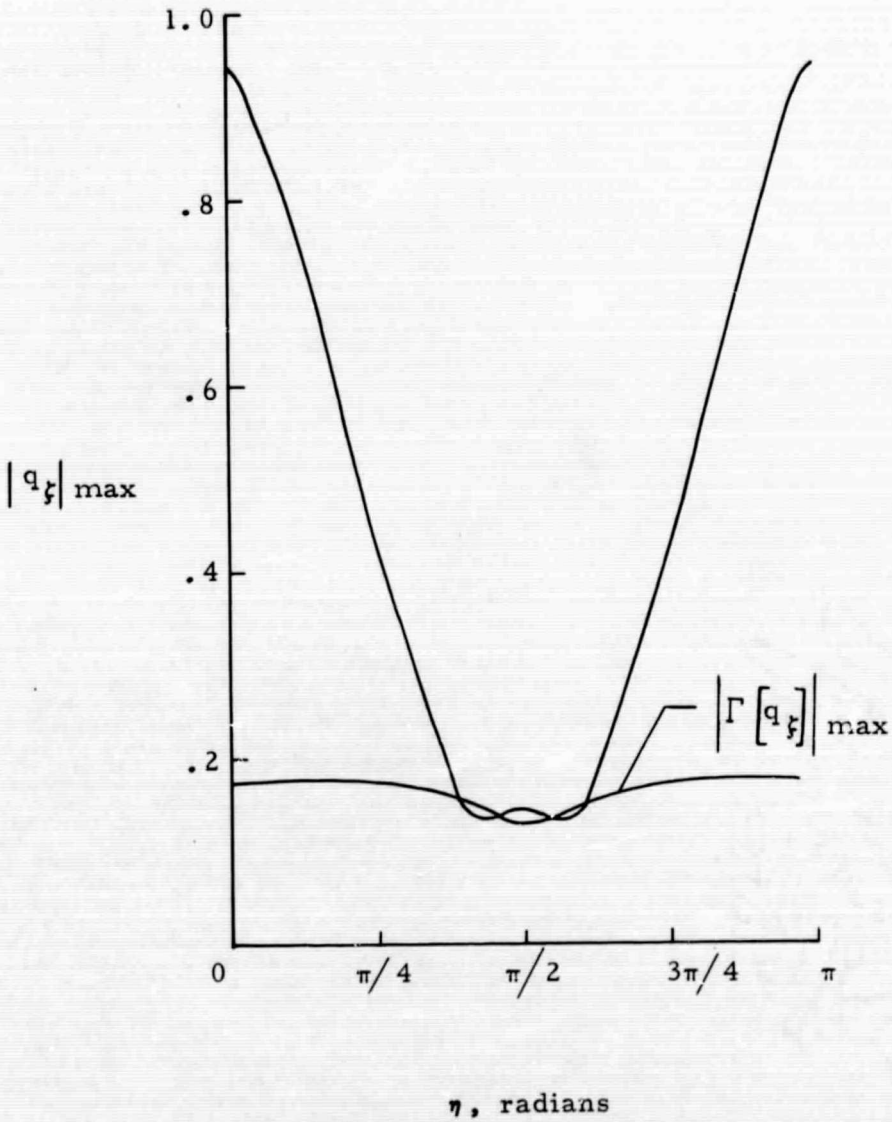

Figure 10.- Velocity amplitude at cylinder surface for grazing wave.

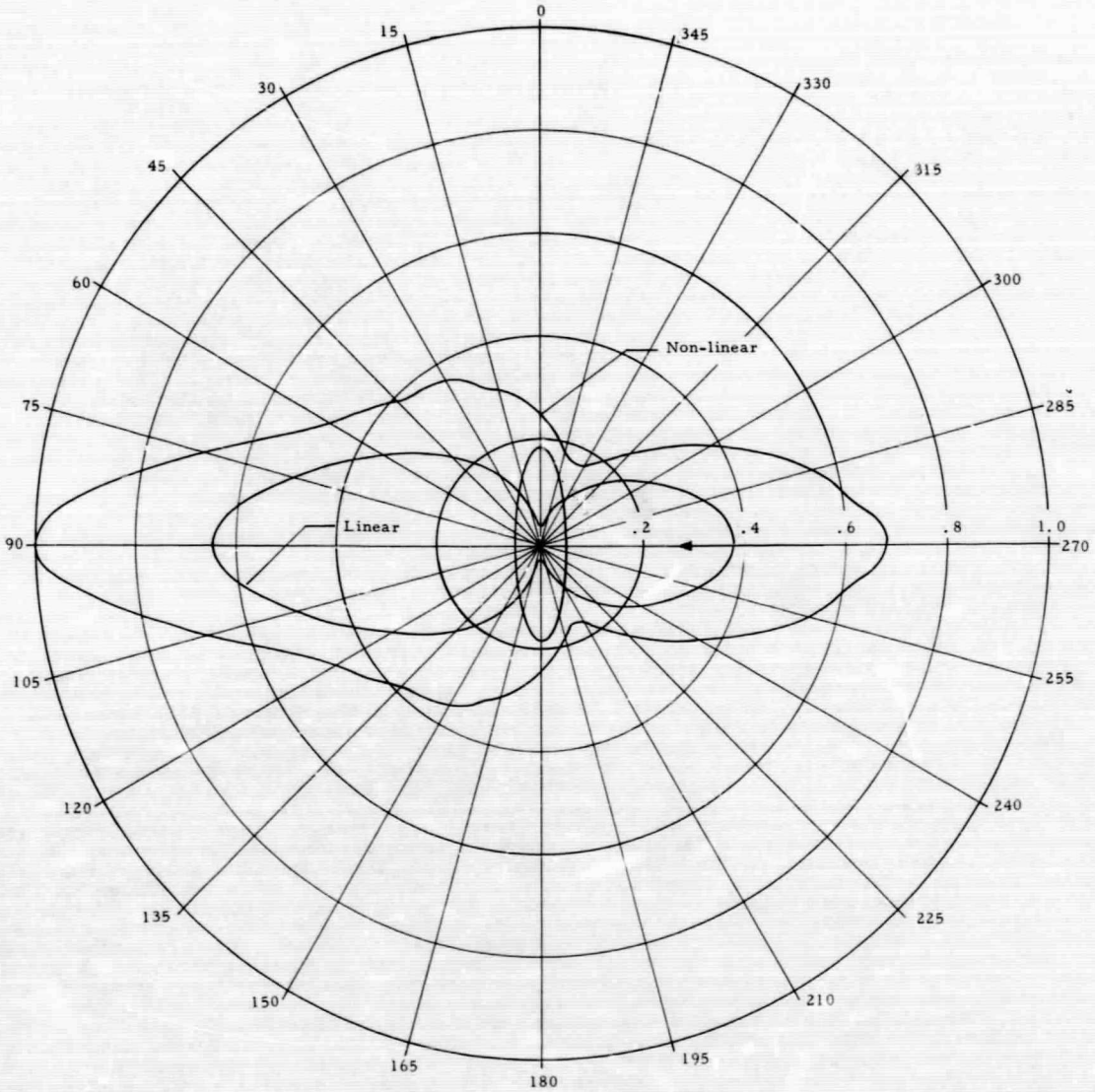

Figure 11.- Normal incidence scattering of a sawtooth wave.

VI. CONCLUDING REMARKS

Integral conservation theorems have been used to derive a set of laws which govern the discontinuities in mass, momentum, and energy flows at a thin sheet of porous material. Each of these laws involve two unknown functions which must be evaluated experimentally. The simplest reasonable approximation to these general laws is made by assuming continuity of normal velocity at the porous surface, and a pressure discontinuity which is a nonlinear function of only the normal velocity. Since this pressure drop is a function of normal velocity, it may be found from a simple steady-state test. It is useful to approximate this nonlinear function by a linear function whose slope depends on the intensity. Deviations from this curve may be represented by a parameter which also depends on the intensity. This approach has been shown to be useful for intensities up to about 160 dB.

The spectral analysis formulation of a one-dimensional problem results in infinite sets of nonlinear equations. These may be solved by an optimization procedure, such as the steepest descent method, for arbitrary nonlinearity or by power series techniques for small nonlinearity. The power series technique is also useful when it is combined with a quasi-linear approximation to the actual nonlinear function.

The temporal formulation of the one-dimensional problem results in a nonlinear integral equation. Numerical approximations to this integral equation again give finite sets of nonlinear algebraic equations to be solved.

Two exact solutions of the one-dimensional problem may be found. These solutions are for a porous sheet mounted in an infinite tube and for a sheet with a rigid quarter-wavelength backing. Both solutions are given in terms of the inverse of a nonlinear algebraic function.

The exact solution for scattering from a porous elliptic cylindrical shell with linear acoustic resistance may be found in terms of Mathieu function series. Coefficients of these series must be found by inversion of four infinite matrices. Elements of these matrices depend on integrals of the periodic Mathieu functions and on the radial Mathieu functions. Series expressions for the integrals have been found. The Mathieu functions may be evaluated in terms of known trigonometric and Bessel function series. By use of highly accurate modern computers, it has been possible to evaluate these functions for a range of parameters where no tables are available. Thus, it has been possible to present results for a range of frequencies where only formal solutions exist in previous literature.

For a special case where the acoustic resistance is a certain function of position on the cylinder, the infinite matrices reduce to diagonal forms, so that simple closed-form expressions in the series solutions are available.

It has been possible to obtain numerical results inside the cylinder, and outside of the cylinder in both the near-field and the far-field. Near-field solutions have been used to obtain the power dissipated in the porous shell.

The power series method has been used to obtain approximate solutions for scattering from a cylinder with nonlinear acoustic resistance. It

has been shown that there may be significant differences between the linear and nonlinear solutions at high intensities.

The exact solution for scattering from a cylinder with large nonlinearity depends on solving doubly-infinite sets of nonlinear algebraic equations. It has been found that computer-time for a power series solution is roughly 100 times as large as for a linear solution. Because of this, it is impractical to solve the problem of large nonlinearity in the spectral domain until more efficient computational programs can be developed.

VII. BIBLIOGRAPHY

1. Marsh, Alan H.: "Study of Acoustical Treatments for Jet-Engine Nacelles." J. Acous. Soc. Am., pp. 43, 5, 1137, 1156, 1968.

2. Mason, W. P. (editor): "Physical Acoustics," vol. 2, part B, ch. 10. Academic Press, 1965.

3. Morse, P. M.; and Ingard, K. U.: "Theoretical Acoustics." McGraw-Hill, 1968.

4. Blackstock, D. T.: "Connection Between the Fay and Fubini Solutions for Plane Sound Waves of Finite Amplitude." J. Acous. Soc. Am., pp. 39, 6, 1019, 1966.

5. Fay, R. D.: "Plane Sound Waves of Finite Amplitude." J. Acous. Soc. Am., pp. 3, 222-241, 1931.

6. Fubini, Ghiron, S.: Alta Frequenza, pp. 4, 530, 1935.

7. Coppens, A. B.; and Saunders, J. V.: "Finite-Amplitude Standing Waves in Rigid-Walled Tubes." J. Acous. Am., pp. 43, 3, 516-529, 1967.

8. Moslen, S. H.; and Moore, F. K.: "On Strong Transverse Waves Without Shocks in a Circular Cylinder." J. of Aero. Sciences, pp. 23, 6, 583-593, 1956.

9. Isakovich, M. A.: "Nonlinear Effects Involved in Certain Acoustical Problems." Soviet Physics-Acoustics," (translantion). pp. 6, 3, 321-325, 1961.

10. Biot, M. A.: "Generalized Theory of Acoustic Propagation in Porous Dissipative Media." J. Acous. Soc. Am., pp. 34, 9, 1254-1264, 1962.

11. Biot, M. A.: "The Mechanics of Deformation and Acoustic Propagation in Porous Media." J. Appl. Phys., pp. 33, 1482-1498, 1962.

12. Comtois, W. H.: "Oblique Flow Losses in Screen Matrix Heat Exchangers." Tech. Rept. No. 29, Dept. of Mech. Eng. Stanford University, Stanford, California, June 1956.

13. London, A. L.; Mitchell, J. W.; and Sutherland, W. A.: "Heat Transfer and Flow Friction Characteristics of Crossed-Rod Matrices." Tech. Rept. No. 41, Dept. of Mech Eng., Stanford University, Stanford, California, July 1959.

14. Wood, Charles C.; and Knip, Gerald, Jr.: "An Investigation of Screens for Removing Distortions in Ducted Flows at High Subsonic Speeds." NACA RM L57G08, 1957.

15. Stokes, George M.; Davis, Don D., Jr.; and Sellers, Thomas B.: "An Experimental Study of Porosity Characteristics of Perforated Materials in Normal and Parallel Flow." NACA TN 3805, 1954.

16. Hoerner, S. F.: "Pressure Losses Across Screens and Grids." Air Force Tech. Rept. No. 6289, Wright-patterson Air Force Base, Dayton, Ohio, 1950.

17. Center, R. E.: "The Interaction of a Rarefaction Wave With a Wire Grid." Rept. A118, Dept. of Supply, Australian Defense Scientific Service Aeronautical Research Laboratories, Melbourne, Australia, 1959.

18. Yates, E. Carson, Jr.: "On the Permeability of Porous Materials." NACA TN 3596, 1956.

19. Pinker, R. A.; and Herbert, M. V.: "The Pressure Loss Associated With Compressible Flow Through Square-Mesh Wire Grids." Rept. R. 281, National Gas Turbine Establishment, Farnborough, United Kingdom.

20. Sivian, L. J.: "Acoustic Impedance of Small Orifices." J. Acous. Soc. Am., pp. 7, 94-101, 1935.

21. Ingard, Uno: "On the Theory and Design of Acoustic Resonators." J. Acous. Soc. Am., pp. 25, 6, 1037-1061, 1953.

22. Bies, David A.; and Wilson, O. B.: "Acoustic Impedance of a Helmholtz Resonator at Very High Amplitude." J. Acous. Soc. Am., pp. 29, 6, 711-714, 1957.

23. Thurston, George B.; Hargrove, Logan E.; and Cook, Bill D.: "Nonlinear Properties of Circular Orifices." J. Acous. Soc. Am., pp. 29, 9, 992-1000, 1957.

24. Ingard, Uno; and Ising, Hartmut: "Acoustic Nonlinearity of an Orifice." J. Acous. Soc. Am., pp. 42, 1, 6-17, 1967.

25. Zorumski, W. E.; and Parrott, Tony L.: "Nonlinear Acoustic Theory for Thin Porous Sheets." NASA SP-189, Conference on Progress of NASA Research Relating to Noise Alleviation of Large Subsonic Jet Aircraft, October 1968.

26. Bouwkamp, C. J.: Rept. Progr. Phys., pp. 17, 35-99, 1954.

27. Yeh, C.: "The Diffraction of Waves by a Penetrable Ribbon." J. Math. Phys., pp. 4, 65-71, 1963.

28. Barakat, R.: "Diffraction of Plane Waves by an Elliptic Cylinder." J. Acous. Soc. Am., pp. 35, 1190-1996, 1963.

29. Burke, James E.: "Low-Frequency Approximations for Scattering by Penetrable Elliptic Cylinders." J. Acous. Soc. Am., pp. 36, 11, 2059-2070, 1964.

30. Barakat, R.; Houston, A.; and Levin, E.: "Power Series Expansion of Mathieu Functions With Tables of Numerical Results." J. Math. Phys., pp. 42, 200-247, 1963.

31. Barakat, R.; Houston, A.; and Levin, E.: "Tables of Moduli and Phase Shifts of the Modified Mathieu Functions and Their Derivatives." Itek Corp. Rept., 1962.

32. Burke, J. E.; and Turersky, V.: "On Scattering of Waves by an Elliptic Cylinder and by a Semielliptic Protuberance on a Ground Plane." J. Opt. Soc. Am., pp. 54, 732-744, 1964.

33. Twersky, F.: "Acoustic Bulk Parameters of Random Volume Distributions of Small Scatters." J. Acous. Soc. Am., pp. 36, 1314-1329, 1964.

34. Wiltse, J. C.; and King, M. J.: "Values of the Mathieu Functions." Johns Hopkins Univ. Rad. Lab. Rept. AF-53, August 1958.

35. Wiltse, J. C.; and King, M. J.: "Derivatives, Zeroes, and Other Data Pertaining to Mathieu Functions." Johns Hopkins Univ. Rad. Lab. Rept. AF-57, December 1958.

36. McLachlan, N. W.: "Theory and Application of Mathieu Functions." Dover Publications, Inc., New York, 1964.

37. Arscott, F. M.: "Periodic Differential Equations." Macmillan Co., New York, 1964.

38. Meixner and Schäfke: "Mathieusche Funktionen und Sphäroidfunktionen." Springer, 1954.

39. Erdilyi, et al.: "Higher Transcendental Functions." Vol. 3, McGraw-Hill, New York, 1955.

40. "Handbook of Mathematical Functions With Formulas, Graphs, and Mathematical Tables." National Bureau of Standards, June 1964.

41. "Tables Relating to Mathieu Functions." Columbia University Press, 1951.

42. "Tables Relating to Mathieu Functions." National Bureau of Standards, August 1967.

43. Kelley, Henry J.: "Methods of Gradients." Ch. 6 of "Optimization Techniques." George Leitmann, editor, Academic Press, New York, 1962.

44. Conway, H. D.: "The Approximate Analysis of Certain Boundary Value Problems." J. Appl. Mech., pp. 27, 275-277, 1960.

45. Swick, D. A.: "Discrete Fourier Transforms a Tutorial Approach." NRL Report 6557, Naval Research Laboratory, Washington, D. C., June 1967.

46. Whittaker, E. T.: "On the Functions Which are Represented by the Expansions of the Interpolation-Theory." Proc. of the Royal Soc. of Edinburg, pp. 35, 181-194, 1914-15.

47. Cooley, James W.; and Tukey, John W.: "An Algorithm for the Machine Calculation of Complex Fourier Series." Math. of Comp., pp. 19, 90, 297-301, 1965.

48. Cochran, William T., et al.: "What is the Fast Fourier Transform?" IEEE Trans. Vol. AU-15, pp. 2, 45-55, 1967.

49. Sneddon, I. N.: "Elements of Partial Differential Equations." McGraw-Hill, New York, 1957.

50. Aczel, J.: "Lectures on Functional Equations and Their Applications." Academic Press, New York, 1966.

51. Watson, G. N.: "A Treatise on the Theory of Bessel Functions." Cambridge University Press, 1966.

52. Hilderbrand, F. B.: "Advanced Calculas for Applications." Prentice-Hall, Inc., 1964.

53. Simeonov, S. V.: "A Method of Solving Systems of Nonlinear Equations of the Potential Type." PMM, pp. 31, 3, 503-508, 1967.

54. Kantorovich, L. V.; and Krylov, V. I.: "Approximate Methods of Higher Analysis." Trans. by Curtiss D. Benster, P. Noordhoff, Ltd., Groningen, The Netherlands, 1958.

55. Blanch, G.: "On the Computation of Mathieu Functions." J. Math. Phys., pp. 25, 1-20, 1946.

56. Stegun, I.; and Abramowitz, M.: "Generation of Bessel Functions on a High Speed Computer." MATC, pp. 11, 255-257, 1957.

57. Blanch, G.; and Clemm, D. S.: "Tables Relating to the Radial Mathieu Functions," vol. 1 and 2. Superintendent of Documents, U.S. Government Printing Office, Washington, D. C., 1962.

VIII. VITA

The author was born in [redacted] on [redacted] [redacted]. In 1957, he entered the University of Missouri School of Mines and Metallurgy and graduated in June 1961 with a B.S. degree in Mechanical Engineering. He then was employed at the Newport News Shipbuilding and Dry Dock Co. until February 1962 when he accepted a position at Langley Research Center. He attended the University of Virginia under Langley's graduate study program and received the Master of Applied Mechanics degree in June 1966. During the 1966-67 academic year, he attended the Virginia Polytechnic Institute and then returned to Langley Research Center where he is currently doing research in acoustics.

IX. APPENDIX

Evaluation of Coupling Coefficients

The integrals defined in equations 4.4(8) and 4.4(9) may be evaluated by expanding the radical in the integrand in a series and then integrating term by term. The integrals to be considered are

$$M_{lr} = \frac{2}{h}\int_0^{2\pi} \frac{Se_l(\eta)Se_r(\eta)d\eta}{\sqrt{2(\cosh 2\xi_o - \cos 2\eta)}} \tag{1}$$

and

$$N_{lr} = \frac{2}{h}\int_0^{2\pi} \frac{So_l(\eta)So_r(\eta)d\eta}{\sqrt{2(\cosh 2\xi_o - \cos 2\eta)}} \tag{2}$$

The radical in the integrand of equations (1) and (2) may be represented as a series of Gegenbaur polynomials. Rainville (51) gives the generating function definition of these polynomials as

$$(1 - 2xt + t^2)^{-\nu} = \sum_{n=0}^{\infty} C_n^{\nu}(x)t^n \tag{3}$$

The denominator of equations (1) and (2) may be written as

$$\left[2(\cosh 2\xi_o - \cos 2\eta)\right]^{-1/2} = \left[e^{2\xi_o}(1 - 2\cos 2\eta\, e^{-\epsilon\xi_o} + e^{-4\xi_o})\right]^{-1/2} \tag{4}$$

Therefore

$$\left[2(\cosh 2\xi_o - \cos 2\eta\right]^{-1/2} = e^{-\xi_o}\sum_{n=0}^{\infty} C_n^{1/2}(\cos 2\eta)\, e^{-2n\xi_o} \tag{5}$$

The Gegenbauer polynomial in equation (5) may be given as (ref. 51, p. 283).

$$C_n^{1/2}(\cos 2\eta) = \sum_{k=0}^{n} \frac{\left(\frac{1}{2}\right)_k \left(\frac{1}{2}\right)_{n-k} \cos 2(n-k)\eta}{k!\,(n-k)!} \tag{6}$$

Equations (5) and (6) combined give the desired expansion for the radical

$$\left[2(\cosh 2\xi_o - \cos 2\eta)\right]^{1/2} = e^{-\xi_o} \sum_{n=0}^{\infty} e^{-2n\xi_o} \sum_{k=0}^{n} \frac{\left(\frac{1}{2}\right)_k \left(\frac{1}{2}\right)_{n-k} \cos 2(n-k)\eta}{k!\,(n-k)!} \tag{7}$$

From equation (7), it may be seen that the integral

$$I_m = \int_0^{2\pi} \frac{\cos m\eta \, d\eta}{\sqrt{2(\cosh 2\xi_o - \cos 2\eta)}} \tag{8}$$

is zero for all odd values of m, consequently, the only integrals which it is necessary to evaluate are of the form

$$I_{2m} = \int_0^{2\pi} \frac{\cos 2m\eta \, d\eta}{\sqrt{2(\cosh 2\xi_o - \cos 2\eta)}} \tag{9}$$

Substituting equation (7) into equation (9) gives

$$I_{2m} = e^{-\xi_o} \sum_{n=m}^{\infty} e^{-2n\xi_o} \sum_{k=0}^{n} \frac{\left(\frac{1}{2}\right)_k \left(\frac{1}{2}\right)_{n-k}}{k!\,(n-k)!} \int_0^{2\pi} \cos 2(n-2k)\eta \cos 2m\eta \, d\eta \tag{10}$$

$$I_{2m} = e^{-(2m+1)\xi_o} \sum_{p=0}^{\infty} \sum_{k=0}^{m+2p} \frac{\left(\frac{1}{2}\right)_k \left(\frac{1}{2}\right)_{(m+2p-k)}}{k!\,(m+2p-k)!} \int_0^{2\pi} \cos 2(m+2p-2k)\eta \cos 2m\eta \, d\eta \tag{11}$$

In equation (11), nonzero terms occur only when $k = p$ or $k = p + m$, therefore,

$$I_{2m} = 2\pi\, e^{-(2m+1)\xi_o} \sum_{p=0}^{\infty} \frac{\left(\frac{1}{2}\right)_p \left(\frac{1}{2}\right)_{p+m}}{p!\ (p + m)!}\, e^{-4p\xi_o} \tag{12}$$

Since the factorial terms in equation (12) form a decreasing sequence, the error due to truncating the series is

$$E < \frac{\left(\frac{1}{2}\right)_N \left(\frac{1}{2}\right)_{N+m}}{N!\ (N + m)!}\, \frac{e^{-4(N-1)\xi_o}}{4\xi_o} \tag{13}$$

A relative measure of the error is obtained by taking the ratio of (13) to the first term in the series for I_{2m}.

$$E_{rel} < \left[\frac{(2m + 1)(2m + 3)\ .\ .\ .(2m + 2N - 1)}{(2m + 2)(2m + 4)\ .\ .\ .(2m + 2N1)}\right] \frac{e^{-4(N-1)\xi_o}}{4\xi_o} \tag{14}$$

Since the first term in the inequality (14) is always less than 1,

$$E_{rel} < \frac{e^{-4\xi_o(N-1)}}{4\xi_o} \tag{15}$$

Then if

$$E_{rel} < 10^{-P} \tag{16}$$

and

$$\xi_o = 10^{-R} \tag{17}$$

an estimate of the number of required terms is

$$N > 10^R(P + R) \tag{18}$$

Thus, for eight significant figures (P = 8), 90 terms are required for $\xi_o = 0.1$, and 1000 terms are required for $\xi_o = 0.01$. With N determined by (18), we put

$$I_{2m} \cong 2\pi\, e^{-(2m+1)\xi_o} \sum_{p=0}^{N} \frac{\left(\frac{1}{2}\right)_p \left(\frac{1}{2}\right)_{p+m}}{p!\,(p+m)!}\, e^{-4p\xi_o} \tag{19}$$

Once the integrals I_{2m} are evaluated, they may be used to evaluate the integrals in equations (1) and (2). First, consider the product of the Mathieu functions in the integrand of equation (1). If se_L and se_r both have period π, their product may be written as

$$Se_{2L}Se_{2r} = \sum_{k=0}^{\infty} \sum_{j=0}^{\infty} De_{2k}^{(2L)}\, De_{2j}^{(2r)} \cos 2k\eta \cos 2j\eta \tag{20}$$

$$\cos 2k\eta \cos 2j\eta = \frac{1}{2} \cos 2(k - j)\eta + \frac{1}{2} \cos 2(k + j)\eta$$

Note that each term in the series is an even multiple of η. Consequently,

$$M_{2L,2r} = \frac{2}{h} \sum_{k=0}^{\infty} \sum_{k=0}^{\infty} De_{2k}^{(2L)}\, De_{2j}^{(2r)} \left(\frac{I_{2|k-j|} + I_{2(k+j)}}{2} \right) \tag{21}$$

The product of Mathieu functions with different periods gives a series whose terms are all odd multiples of η. It was noted in equation (8) that the integral of these terms is zero, therefore,

$$M_{2L+1,2r} = 0 \tag{23a}$$

$$M_{2L,2r+1} = 0 \tag{23b}$$

The product of even Mathieu functions with period 2π is

$$Se_{2L+1}, Se_{2r+1} = \sum_{k=0}^{\infty} \sum_{j=0}^{\infty} De_{2r+1}^{(2L+1)} \; De_{2j+1}^{(2r+1)} \cos (2k + 1)\eta \cos (2j + 1)\eta \tag{24}$$

Therefore

$$M_{2L+1,2R+1} = \frac{2}{h} \sum_{k=0}^{\infty} \sum_{j=0}^{\infty} De_{2k+1}^{(2L+1)} \; De_{2j+1}^{(2r+1)} \left(\frac{I_{2|k-j|} + I_{2(k+j+1)}}{2} \right) \tag{25}$$

A similar evaluation for integrals involving odd Mathieu functions gives

$$N_{2L+1,2r+1} = \frac{2}{h} \sum_{k=0}^{\infty} \sum_{j=0}^{\infty} Do_{2k+1}^{(2L+1)} \; Do_{2j+1}^{(2r+1)} \left(\frac{I_{2|k-j|} - I_{2(k+j+1)}}{2} \right) \tag{26}$$

$$N_{2L+2,2r+2} = \frac{2}{h} \sum_{k=0}^{\infty} \sum_{j=0}^{\infty} Do_{2k+2}^{(2L+2)} \; Do_{2j+2}^{(2r+2)} \left(\frac{I_{2|k-j|} - I_{2(k+j+2)}}{2} \right) \tag{27}$$